

Dipolar interaction and demagnetizing effects in magnetic nanoparticle dispersions: Introducing the mean-field interacting superparamagnet model

F. H. Sánchez,^{1,*} P. Mendoza Zéllis,^{1,2} M. L. Arciniegas,¹ G. A. Pasquevich,^{1,2} and M. B. Fernández van Raap¹

¹*IFLP-CCT-La Plata-CONICET and Departamento de Física, Facultad de Ciencias Exactas, C.C. 67, Universidad Nacional de La Plata, 1900 La Plata, Argentina*

²*Departamento de Ciencias Básicas, Facultad de Ingeniería, Universidad Nacional de La Plata, 1900 La Plata, Argentina*

(Received 8 June 2016; revised manuscript received 21 February 2017; published 13 April 2017)

Aiming to analyze relevant aspects of interacting magnetic nanoparticle systems (frequently called interacting superparamagnets), a model is built from magnetic dipolar interaction and demagnetizing mean-field concepts. By making reasonable simplifying approximations, a simple and useful expression for effective demagnetizing factors is achieved, which allows the analysis of uniform and nonuniform spatial distributions of nanoparticles, in particular the occurrence of clustering. This expression is a function of demagnetizing factors associated with specimen shape and clusters shape, and of the mean distances between near neighbor nanoparticles and between clusters, relative to the characteristic sizes of each of these two types of objects, respectively. The model explains effects of magnetic dipolar interactions, such as the observation of apparent nanoparticle magnetic moments smaller than real ones and approaching to zero as temperature decreases. It is shown that by performing a minimum set of experimental determinations along principal directions of geometrically well-defined specimens, model application allows retrieval of nanoparticle intrinsic properties, like mean volume, magnetic moment, and susceptibility in the absence of interactions. It also permits the estimation of mean interparticle and intercluster relative distances, as well as mean values of demagnetizing factors associated with clusters shape. An expression for average magnetic dipolar energy per nanoparticle is also derived, which is a function of specimen effective demagnetizing factor and magnetization. Experimental test of the model was performed by analysis of results reported in the literature and of original results reported here. The first case corresponds to oleic-acid-coated 8-nm magnetite particles dispersed in PEGDA-600 polymer, and the second one to polyacrylic-acid-coated 13-nm magnetite particles dispersed in PVA solutions from which ferrogels were later produced by a physical cross-linking route. In both cases, several specimens were studied covering a range of nanoparticle volume fractions between 0.002 and 0.046. Magnetic response is clearly different when prism-shaped specimens are measured along different principal directions. These results remark the importance of reporting complete information on measurement geometry when communicating magnetic measurement results of interacting magnetic nanoparticles. Intrinsic nanoparticle properties as well as structural information on particles spatial distribution were retrieved from our analysis in addition to, and in excellent agreement with, analysis previously performed by other authors and/or information obtained from FESEM images. In the studied samples, nanoparticles were found to be in close contact to each other within almost randomly oriented clusters. Intercluster mean distance, relative to cluster size, was found to vary between 2.2 and 7.5, depending on particles volume fraction.

DOI: [10.1103/PhysRevB.95.134421](https://doi.org/10.1103/PhysRevB.95.134421)

I. INTRODUCTION

A. Motivation

Magnetic nanoparticles (NPs) and their solid and liquid dispersions are the subject of intense research due to their interesting basic properties and their potential applications in several fields as catalysis, biomedicine, environment, space, and industry [1–6]. Magnetic NPs present unique properties, i.e., single-domain state, large resultant magnetic moment, moment relaxation mechanisms specific to the nanoscale, magnetic anisotropy strongly affected by shape and surface, etc. [7,8]. In addition, all these properties can be strongly modified by interactions between particles [9–15].

A continuous magnetic material having nonzero magnetization gives rise to a dipolar field originated in its elemental magnetic moments. Outside the material, the dipolar field is

known as stray field, which allows the detection and measurement of the specimen magnetic moment in magnetometer and susceptometer devices. Inside the material, the average dipolar field at a given point is related to average magnetization by a tensor known as demagnetizing tensor. For any uniformly magnetized specimen, there are three principal directions \hat{u} for which the inner average dipolar field \vec{H}^D opposes average magnetization \vec{M} and is referred to as demagnetizing field. In such simplest case \vec{H}^D is a mean field proportional to $-\vec{M}$ through a demagnetizing factor N_{su} ($\vec{H}^D = -N_{su}\vec{M}$), which depends on specimen (s) geometry and on measurement direction \hat{u} . In this reference frame, the demagnetizing field tensor is diagonal and its trace is unity in SI units system [16,17], $\sum_u N_{su} = 1$.

If the specimen is under an external applied field \vec{H}^A , the effective average field \vec{H}^E within it has a reduced value because of the demagnetizing field presence, being $\vec{H}^E = \vec{H}^A + \vec{H}^D$. Due to this fact, its apparent low-field susceptibility $\kappa_u = \left. \frac{\partial M_u}{\partial H_u^A} \right|_{H_u^A=0}$ is lower than its actual or true

*sanchez@fisica.unlp.edu.ar

susceptibility $\chi_u = \frac{\partial M_u}{\partial H_u^E} |_{H_u^E=0}$, then

$$\kappa_u = \chi_u / (1 + N_{su} \chi_u). \quad (1)$$

A ferro- or ferrimagnetic NP is a continuous piece of single-phase material. Below a critical size the NP is a single-domain and consequently bears a magnetization equal to its spontaneous magnetization M^S , which depends on temperature. Demagnetizing field originated in NP magnetization creates magnetic anisotropy. This anisotropy, which depends on the form of the NP, is a function of its demagnetizing tensor and is known as shape anisotropy. Commonly principal contributions to anisotropy in magnetic NPs come from NP shape, crystalline structure, and surface. In magnetostrictive materials, applied stress needs to be considered as another source of anisotropy. Usually the combined effect of all potential causes can be described by an effective uniaxial anisotropy K [18].

In this work we present a model to describe how magnetic dipolar interactions modify the response of an ensemble of particle moments to an applied magnetic field. It is known that interactions change magnetic response in general [9–15]. In particular they modify susceptibility, relaxation time, and coercivity. They may also lead to a collective behavior of the ensemble of moments, in cases giving rise to freezing of the system as a whole, when temperature is reduced below a critical value [19]. Even at temperatures where the system behaves as an interacting superparamagnet [20], i.e., where the particle-moment relaxation-time is shorter than observation time and the magnetic measurements display features of an equilibrium process, experimentally retrieved functions of temperature and applied field, like susceptibility and magnetization, may result in being considerably affected by dipolar interactions. In such cases, it is remarkable that while the magnetization can still be described using the same functions, which are valid in the absence of interactions (like Langevin and hyperbolic tangent functions, for example), function parameters do not correspond to real physical properties of the particles. This is the case of particle magnetic moments, which may display apparent values approaching zero as temperature decreases [20,21]. Allia *et al.* [20] proposed a simple model that has proven to be successful for analyzing some particular cases of the situation just mentioned. In that model, dipolar energy per particle is written as $\varepsilon = \alpha \mu_0 \langle \mu \rangle^2 / 4\pi d^3$, α being a geometrical factor [22], $\langle \mu \rangle$ the particle mean-magnetic-moment, and d the mean distance between centers of near neighbor particles. Dipolar energy is equated to a typical thermal energy kT^* , where T^* is a model parameter representing the temperature that must be added to actual temperature T in the argument of the theoretical equilibrium function, in order to give a correct description of the material response and properties.

Recently [23,24], it has been reported that when magnetic entities dispersed in a nonmagnetic matrix strongly interact with each other, sample structure plays a role in defining easy and hard directions. This effect is clearly observed in self-organized magnetic nanowire arrays in alumina matrices. In these works metallic nanowires constituted by nanoparticles are grown in alumina membranes forming a bidimensional network, pointing parallel to each other and perpendicular to the specimen plane. Typically, nanowires are a few tens of nm wide and a few μm long, while the alumina film has a few

nm^2 area. Separation between nanowires is of the order of 1.7 to 3 times the nanowire diameter. When the separation-to-diameter-ratio decreases and dipolar interaction between nanowires increases, the effective magnetization easy direction rotates from the nanowire longitudinal axis toward an axis parallel to the film, i.e., from the nanowire easy direction to the film easy one [23,24].

One question emerging from this scenario is whether dipolar interactions in magnetic nanodispersions can be described through an internal demagnetizing mean field affected by specimen shape and the spatial distribution of NPs. For example, when magnetic nanoparticles are not uniformly distributed but are arranged in clusters or display spatial concentration fluctuations: could this problem be treated using demagnetizing factors associated to the specimen and clusters geometries? The problem is complicated because clusters may vary in shape, size, spatial distribution, and NPs concentration [14]. Besides, magnetization is never uniform at a sufficiently reduced scale. The purpose of this paper is to explore how this question can be answered, what approximations must be done, and what limitations appear. We anticipate that under certain conditions, which are frequently realized in experimental scientific work related to solid magnetic particle dispersions, the response to this question is affirmative. On the other hand, in liquid dispersions NPs are free to move and form structures with low (negative) dipolar energy, as for example chains where these linear arrays and moments of NPs contained in them align preferentially in the direction of the applied field, thus leading to magnetizing rather than to demagnetizing effects [25].

After reviewing concepts about magnetic susceptibility in Sec. IB, which are relevant for the model formulation and its application, in Secs. IIA–IID we will develop the model and the strategies to extract useful information on parameters that characterize the NPs spatial distribution. The present work provides solid bases for the understanding of the effect of dipolar interactions in dispersions of magnetic single-domain objects. We will discuss the most relevant similarities and differences with other descriptions reported in the literature and discuss a few examples of analysis applied to published and unpublished results. We will show that meaningful information can be retrieved even when the knowledge of some experimental details is missing. Finally, we will suggest convenient measurement protocols that can be followed in order to efficiently retrieve such information.

B. Considerations about magnetic susceptibility of noninteracting NPs

At this point we consider it is necessary to remind the reader of the dependence of low-field susceptibility of an ensemble of identical anisotropic noninteracting NPs of volume V , on easy axes orientations, temperature, and measurement time. To this end, it is convenient to start with a phenomenological model for the complex susceptibility [26],

$$\chi_u = \frac{\chi_{u0} + i \chi_{u\infty} \tau / \tau_{\text{exp}}}{1 + i \tau / \tau_{\text{exp}}}, \quad (2)$$

where τ is the NP moment relaxation time, τ_{exp} is the measurement time, χ_{u0} is the equilibrium susceptibility,

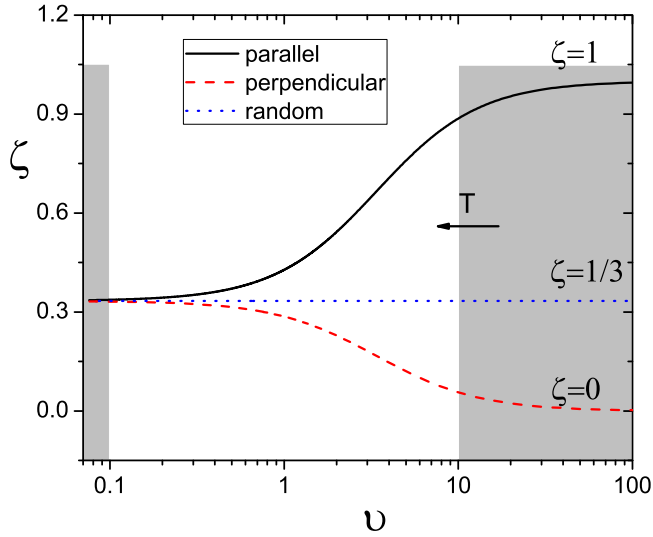


FIG. 1. Ratio $\zeta_u(\nu, \theta) = \chi_{u0}/(3\chi_L)$ for different orientation of easy axes relative to applied field direction. Shaded regions correspond to $\nu \ll 1$, where the distribution of easy axes orientations is irrelevant, and to $\nu \gg 1$, where this distribution plays a crucial role.

valid when $\tau/\tau_{\text{exp}} \rightarrow 0$, and $\chi_{u\infty}$ is the susceptibility far from equilibrium, i.e., when $\tau/\tau_{\text{exp}} \rightarrow \infty$. When $\tau/\tau_{\text{exp}} = 1$, blocking of magnetic moment occurs, and this happens at a temperature referred to as blocking temperature T_b .

χ_{u0} depends on temperature, on the ratio of anisotropy to thermal energies $\nu = KV/kT$, and on the angle θ between easy axis and the direction of the applied field (which is also the measurement direction). It is convenient to express χ_{u0} in terms of the Langevin susceptibility corresponding of NPs without anisotropy, $\chi_L = \frac{\mu_0\mu^2}{3VkT}$, as

$$\chi_{u0}(\nu, \theta) = 3\zeta_u(\nu, \theta)\chi_L, \quad (3)$$

where $\zeta_u(\nu, \theta)$, the ratio $\chi_{u0}/(3\chi_L)$, has been recently obtained [27] in terms of the imaginary error function of ν . A useful simple expression for $\zeta_u(\nu, \theta)$ can be derived partially from an approximated expression reported in Ref. [28] for the case $\theta = 0$,

$$\zeta_u(\nu, \theta) \approx \frac{(\nu/3.4)^{1.47} \cos^2(\theta) + 1/3}{(\nu/3.4)^{1.47} + 1}. \quad (4)$$

At sufficiently high temperatures, when $\nu \ll 1$, the equilibrium susceptibility does not depend on θ , $\chi_0(\nu \ll 1, \theta) = \chi_L$. On the other hand, at sufficiently low temperatures, when $\nu \gg 1$, $\zeta_u(\nu, \theta) \approx \cos^2(\theta)$ and the equilibrium susceptibility becomes $\chi_0 = 3\cos^2(\theta)\chi_L$. For an ensemble of NPs whose easy axes are randomly oriented, $\chi_0 = \chi_L$ holds in the whole temperature range. Indeed, Eq. (4), represented in Fig. 1, reproduces very well the dependence of χ_0 with ν and θ semiquantitatively shown in Ref. [29]. Equation (4) provides a quantitative tool to treat the general case of any arbitrary orientation of easy axis relative to the applied field direction at any temperature. Notice that even at room temperature $\zeta_u(\nu, \theta)$ values corresponding to typical NPs (10-nm diameter and $K = 2 \times 10^4 \text{ J/m}^3$, $\nu \approx 2.53$) display a quite important dependence on particle orientation (see vertical line in Fig. 1).

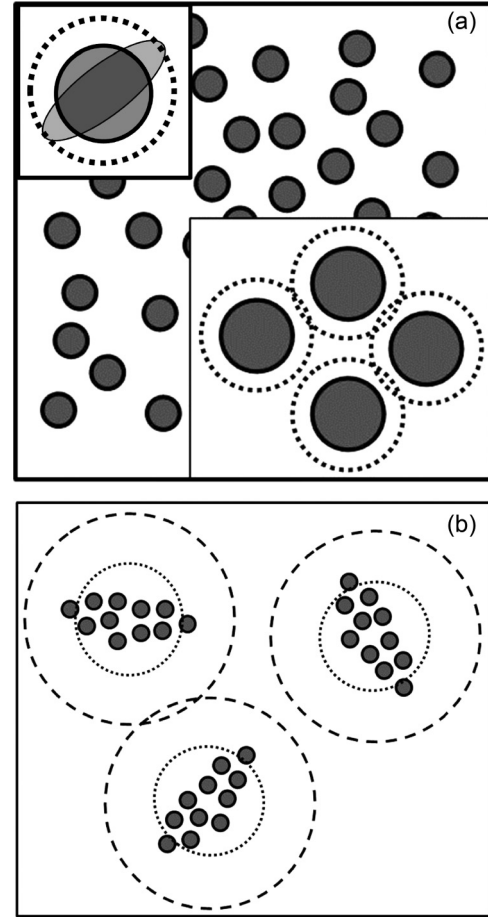


FIG. 2. Sketch of nanoparticles and clusters. (a) Left-top inset: NP shape (ellipse), sphere of diameter D with same volume V as NP (continuous contour), and sphere with diameter equal to mean near-neighbor distance $d = \gamma D$ (dotted contour, see also right-bottom inset). Main figure: random distribution of NPs in a nonmagnetic matrix. Packing fraction of dotted spheres is ϕ . (b) Nonrandom distribution of NPs. Dotted spheres of diameter D_c have same volume V_c as clusters. Mean distance between near-neighbor clusters is $d_c = \gamma_c D_c$. Dashed spheres diameter is d_c . Packing fraction of dashed spheres is ϕ_c .

II. MODEL

A. Demagnetizing field and demagnetizing factors

Let us consider a three-dimensional spatial distribution of identical magnetic NPs in a nonmagnetic matrix. Such a distribution may be in states of higher complexity than uniformity or randomness [Fig. 2(a)]. We will only consider the cases in which spatial fluctuations of the number of particles per volume unit can be accounted by the existence of identical NP clusters [Fig. 2(b)]. Such clusters are specimen regions where NPs are located.

In order to relate volumes of NPs, clusters, and specimen, we will make a few simplifying assumptions. To this end, each NP volume V is represented by a sphere of diameter D with the same volume. Similarly, volume V_c of NPs clusters will be represented by that of spheres of diameter D_c . We introduce two parameters, $\gamma = d/D$, the near-neighbor mean interparticle-distance d relative to D ; and $\gamma_c = d_c/D_c$, the near-neighbor mean intercluster-distance (center to center) d_c

relative to D_c . We define the NP packing fraction φ as the ratio of volume associated to all of the NPs within a cluster to the cluster volume, where the volume associated to one NP is defined as that of a sphere of diameter d . Hence, $\varphi = n_{pc}\gamma^3 D^3/D_c^3$ [see Fig. 2(a)], where n_{pc} is the number of NPs per cluster.

Dipolar field at the position of NP i generated by the other NPs (j) is a function of moments $\vec{\mu}_j = \mu \hat{v}_j$, and vectors $\vec{d}_{ij} = d_{ij} \hat{u}_{ij}$, which are the positions of NPs j relative to NP i , where \hat{v}_j and \hat{u}_{ij} are unitary vectors, and is given by

$$\vec{H}_i^D = \frac{\mu}{4\pi} \sum_{j \neq i}^{n_{ps}} \vec{s}_{ij}/d_{ij}^3,$$

where $\vec{s}_{ij} = 3(\hat{v}_j \cdot \hat{u}_{ij})\hat{u}_{ij} - \hat{v}_j$ and n_{ps} is the total number of NPs in the specimen. This expression is strictly valid for spherical single-domain NPs, which generate a disperse magnetic field identical to that of magnetic dipoles of intensity $\mu = VM^S$. It is still a very good approximation for NPs not strictly spherical at distances $d_{ij} > nD$, with n of the order of unity [30]. The last equation can be separated in two contribution to the demagnetizing field corresponding to the summations over the n_{pc} NPs inside cluster I , which contains NP i , and over the $n_{ps} - n_{pc}$ remaining NPs inside other clusters,

$$\begin{aligned} \vec{H}_i^D &= \vec{H}_{i,I}^D + \vec{H}_{i,Q \neq I}^D \\ &= \frac{\mu}{4\pi} \sum_{j \neq i}^{n_{pc}} \frac{\vec{s}_{ij}^{II}}{(d_{ij}^{II})^3} + \frac{\mu}{4\pi} \sum_{Q \neq I}^{n_{cs}} \sum_{j=1}^{n_{pc}} \frac{\vec{s}_{ij}^{IQ}}{(d_{ij}^{IQ})^3}, \end{aligned} \quad (5)$$

where n_{cs} is the number of clusters in the specimen, and now d_{ij}^{IQ} and \vec{s}_{ij}^{IQ} are determined for particle i located in cluster I and particle j located in cluster Q . In order to achieve a useful description depending on just a few parameters we will make an approximation in the second summation. We assume that for the evaluation of Eq. (5) it is acceptable to assign the value d_{IQ} to the element d_{ij}^{IQ} , where d_{IQ} is the distance between clusters I and Q , center to center. The relative error introduced by this procedure is a decreasing function of d_{IQ} . In order to evaluate its reasonableness we explore the most unfavorable case, which is that of near-neighbor clusters, where the relative error is $\delta = |(1/d_{ij}^3) - 1/d_c^3|/(1/d_c^3)$. δ was calculated for clusters with maximum and minimum anisotropy. Considered cases are spheres [case (a) in Fig. 3] and wires with two different relative orientation [cases (b) and (c) in Fig. 3]. For wires δ was evaluated analytically and for spheres a numerical calculation involving 10^4 NPs randomly distributed per cluster was performed. Results demonstrate that δ is a rapid decreasing function of γ_c and that reduces below 0.1 for $\gamma_c \approx 3.3$ in case (c) and for $\gamma_c \approx 1.7$ in case (a). When Eq. (5) is evaluated, taking into account contributions from all clusters, the relative error in \vec{H}^D is much lower than δ .

Now, we define the nondimensional quantities:

$$\begin{aligned} \vec{\lambda}_i &= \frac{d^3}{n_{pc} - 1} \sum_{j \neq i}^{n_{pc}} \frac{\vec{s}_{ij}^{II}}{(d_{ij}^{II})^3} \quad \text{and} \\ \vec{\lambda}_{ci} &= \frac{d_c^3}{n_{ps} - n_{pc}} \sum_{Q \neq I}^{n_{cs}} \frac{1}{d_{IQ}^3} \sum_{j=1}^{n_{pc}} \vec{s}_{ij}^{IQ}. \end{aligned}$$

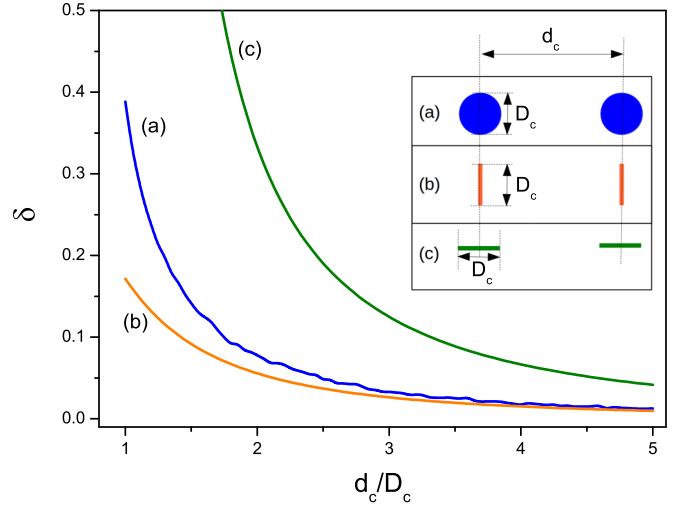


FIG. 3. δ as a function of $\gamma_c = d_c/D_c$ for the case of spheres (a) and wires (b) and (c) with the orientation sketched in the inset.

$\vec{\lambda}_i$ and $\vec{\lambda}_{ci}$ are invariant under similarity transformations performed either on NPs within clusters, or on clusters within the specimen, respectively; a similarity transformation being understood as an isotropic expansion or contraction. $\vec{\lambda}_i$ and $\vec{\lambda}_{ci}$ definitions permit us to write $\vec{H}_{i,I}^D$ and $\vec{H}_{i,Q \neq I}^D$ in more compact form,

$$\begin{aligned} \vec{H}_{i,I}^D &= \frac{\mu}{4\pi} \frac{n_{pc} - 1}{\gamma^3 D^3} \vec{\lambda}_i, \\ \vec{H}_{i,Q \neq I}^D &= \frac{\mu}{4\pi} \frac{n_{ps} - n_{pc}}{\gamma_c^3 D_c^3} \vec{\lambda}_{ci}. \end{aligned}$$

Averaging over the specimen and considering the special case where the specimen magnetization \vec{M}_s lays along one principal direction

$$\begin{aligned} \vec{H}^D &= \langle \vec{H}_i^D \rangle = \vec{H}_{c,int}^D + \vec{H}_{c,ext}^D \\ &= \frac{1}{24} \left(\frac{n_{pc} - 1}{\gamma^3} \vec{\lambda} + \frac{(n_{cs} - 1)\varphi}{\gamma^3 \gamma_c^3} \vec{\lambda}_c \right) M^S \\ &= -N_{su}^E \vec{M}_s, \end{aligned} \quad (6)$$

where $\vec{H}_{c,int}^D = \langle \vec{H}_{i,I}^D \rangle$ and $\vec{H}_{c,ext}^D = \langle \vec{H}_{i,Q \neq I}^D \rangle$ are the mean demagnetizing field generated inside a cluster due to internal and external NPs to this cluster, respectively. In the penultimate member of Eq. (6) we have used $\mu = VM^S$, and we have written $\langle \vec{\lambda}_i \rangle = \vec{\lambda}$, $\langle \vec{\lambda}_{ci} \rangle = \vec{\lambda}_c$, for simplicity. In the last member of Eq. (6) we have introduced two quantities, \vec{M}_s and N_{su}^E . \vec{M}_s is the specimen magnetization defined as the total magnetic moment divided by specimen volume. N_{su}^E is defined as the specimen effective demagnetizing factor, and it is determined by the spatial distribution of NPs in the whole specimen and by the principal direction \hat{u} at which magnetic field is applied and measurement is performed.

Next, based on magnetostatic considerations, we will write \vec{H}^D as a function of demagnetizing factors N_{cu} and N_{su} , corresponding to cluster and specimen shapes; when measurement is performed in the principal direction \hat{u} . Therefore, we will assume that N_{su} and N_{cu} satisfy all properties of magnetostatic demagnetizing factors previously defined in the literature [17].

In this sense, it is useful to introduce the cluster magnetization M_c and the magnetic phase magnetization M , which are defined as the total magnetic moment divided either by the total volume of clusters or by the total volume of NPs. M_s , M_c , and M are related among themselves by

$$M_c = \frac{\varphi}{\gamma^3} M \quad \text{and} \quad M_s = x_V M = \frac{\varphi \varphi_c}{\gamma^3 \gamma_c^3} M, \quad (7)$$

where x_V is the NPs volume fraction in the specimen and φ_c is the clusters packing fraction defined as the ratio of the volume associated to all clusters relative to the specimen volume, where the volume associated to one cluster is defined as that of a sphere of diameter d_c .

Taking into account that $\vec{H}_{c,\text{int}}^D$ is the mean demagnetizing field inside one cluster originated only from the nanoparticles inside this cluster, from magnetostatic considerations this quantity can be written as

$$\vec{H}_{c,\text{int}}^D = -N_{cu} \vec{M}_c. \quad (8)$$

The demagnetizing field originated from NPs outside this cluster, $\vec{H}_{c,\text{ext}}^D$, can be calculated as the demagnetizing field produced by the whole specimen having an average magnetization M_s , minus the demagnetizing field corresponding to the cluster shape if it had the same magnetization M_s , i.e.:

$$\vec{H}_{c,\text{ext}}^D = -(N_{su} \vec{M}_s - N_{cu} \vec{M}_s). \quad (9)$$

From Eq. (6), Eq. (8), and Eq. (9) it is possible to obtain expressions for λ , λ_c :

$$\bar{\lambda} = -24 \frac{\varphi}{n_{pc} - 1} N_{cu} \frac{\vec{M}}{M^S}, \quad (10a)$$

$$\bar{\lambda}_c = -24 \frac{\varphi \varphi_c}{n_{cs} - 1} (N_{su} - N_{cu}) \frac{\vec{M}}{M^S}, \quad (10b)$$

and also for specimen effective demagnetizing factor N_{su}^E . It may be more convenient, for practical purposes, to define the magnetic-phase effective demagnetizing factor N_u^E , which defines \vec{H}^D in terms of the NP magnetization \vec{M} : $\vec{H}^D = -N_u^E \vec{M}$. This choice is justified by the fact that frequently an estimation of $M(H)$ can be more easily made, including the dependence of M^S on NP size [31]. Therefore, the expressions for effective demagnetizing factors, for magnetic phase and specimen, are the following:

$$N_u^E = \frac{\varphi}{\gamma^3} \left(N_{cu} \left(1 - \frac{\varphi_c}{\gamma_c^3} \right) + N_{su} \frac{\varphi_c}{\gamma_c^3} \right), \quad (11a)$$

$$N_{su}^E = \left(\frac{\gamma_c^3}{\varphi_c} - 1 \right) N_{cu} + N_{su}. \quad (11b)$$

Note that $N_u^E = x_V N_{su}^E$.

By construction N_u^E (and N_{su}^E) result from averaging \vec{H}^D and \vec{M} (or \vec{M}_s) over the specimen, therefore they should be considered magnetostatic demagnetizing factors [17] but with the peculiarity of having been defined for a magnetic discontinuous system. In this system, magnetic charges are not located only at specimen surfaces (as it happens in a uniformly magnetized body) since internal charges at NPs surfaces do not cancel completely [14]. Therefore, Eqs. (11) must be carefully

confronted with experimental results in order to determine their usefulness and practical limitations (see Sec. III). N_u^E and N_{su}^E are simple functions of the specimen and cluster demagnetizing factors and of the relative distances γ and γ_c . Since N_{su} and N_{cu} verify $\sum_u N_{su} = \sum_u N_{cu} = 1$, trace of effective demagnetizing tensors become

$$\text{Tr}(N^E) = \frac{\varphi}{\gamma^3}, \quad (12a)$$

$$\text{Tr}(N_s^E) = \frac{\gamma_c^3}{\varphi_c}, \quad (12b)$$

satisfying $\text{Tr}(N^E) = x_V \text{Tr}(N_s^E)$. While frequently N_{su} can be precisely known, in most cases N_{cu} is unknown. However, in some cases its average value over the specimen can be estimated. For example, when clusters are randomly oriented, or at least isotropically, the specimen average value of N_{cu} becomes $N_{cu} = 1/3$.

We will consider three particular cases or limit situations: (i) clusters that do not interact with each other, (ii) clusters in contact with each other, and (iii) nanoparticles that do not interact with each other.

Case (i): The case in which clusters do not interact corresponds to the case in which the distance between cluster is large, i.e., $\gamma_c \rightarrow \infty$. In this case effective demagnetizing factor responds to cluster shape, $N_u^E = \frac{\varphi}{\gamma^3} N_{cu}$, since dipolar interactions are meaningful just within clusters.

Case (ii): When the nanoparticles are homogeneously distributed in the whole specimen there are no clusters, that correspond to $\gamma_c = 1$ and $\varphi_c = 1$. In this case, the effective demagnetizing factors become $N_u^E = \frac{\varphi}{\gamma} N_{su} = x_V N_{su}$ and $N_{su}^E = N_{su}$. The demagnetizing factor is determined just by the specimen geometry.

Case (iii): When particles are very far apart, i.e., when $\gamma \rightarrow \infty$, dipolar interactions among them become negligible and $H^D = -N_u^E M = N_{su}^E M_s$ tends to zero. This happens because $N_u^E = 0$ and $M_s = 0$.

Equation (11a) shows similarities with Eq. (2) of Ref. [14] but a main difference. The expression in Ref. [14] includes an additional term that we may rewrite here as $N_{pu}(1 - x_{Vc})$, where N_{pu} is the demagnetizing factor corresponding to NP shape and x_{Vc} is the volume fraction of NPs in clusters. When multiplied by M , this term gives the part of the average field inside a NP, which is produced by uncompensated magnetic charges at its surface. Equations (11) have been built to describe the mean dipolar field acting on the NPs, not inside them, and therefore should not include such a term. As stated in Sec. IA the effect of the demagnetizing field originating from a NP's own magnetization is taken into account in the effective magnetic anisotropy through the magnetostatic anisotropy contribution.

Recently, an experimental study [15] of dense assemblies (packed powder) of spherical ferrimagnetic NPs, which correspond to our case (ii), was presented. The authors identify effects of the demagnetizing field in temperature-dependent susceptibility curves, which were treated using an approach similar to that of Ref. [14]. Also, the authors have demonstrated how the packing fraction may be determined with this approach.

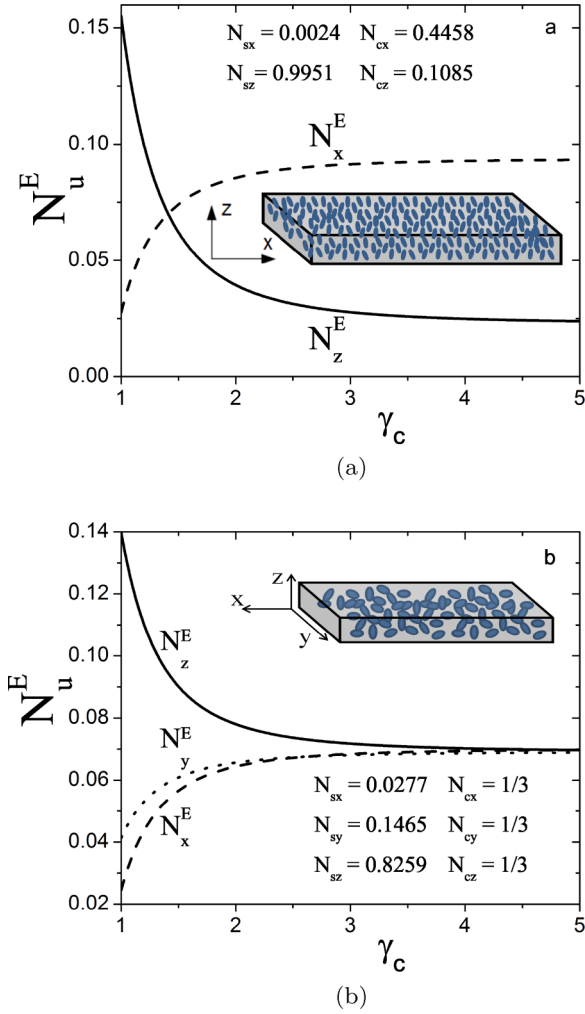


FIG. 4. (a) N_x^E , N_z^E for the case of clusters preferentially oriented. Specimen l_x and l_y dimensions are identical. (b) N_x^E , N_y^E , and N_z^E for a high aspect ratio specimen with clusters randomly oriented. In both examples the NPs relative distance parameter was set at $\gamma = 1.5$.

To end this section we will illustrate the behavior of N_u^E as a function of γ_c with a couple of examples for which $\gamma = 1.5$ was arbitrarily set. For the arrays considered, $\varphi = \varphi_c = 0.7$ was chosen (see Sec. II C). Figure 4(a) corresponds to a distribution of identical ellipsoidal clusters whose easy axes are preferentially oriented perpendicular to the specimen plane (dimensions of specimen satisfy $l_x = l_y \gg l_z$). Model predicts that at $\gamma_c \approx 1.41$ the effective easy direction changes from the cluster easy axis (z) to a direction contained within the plane. In this situation the system presents isotropic demagnetizing properties: $N_x^E = N_y^E = N_z^E \approx 0.070$. Figure 4(b) shows N_x^E , N_y^E , and N_z^E for a specimen with high aspect ratio ($l_x \gg l_y \gg l_z$) and randomly oriented clusters.

B. Demagnetizing field and apparent particle magnetic moment

Let us consider an ensemble of unblocked NPs with a distribution of magnetic moments $f(\mu)$. $f(\mu)d\mu$ is the probability of finding a NP with its moment in the interval $(\mu,$

$\mu + d\mu)$. It is normalized to unity in the interval $(0, \infty)$. For simplicity we will assume M^S independent of NP size, hence $\mu = M^S(T)V$. When there are no interparticle interactions the ensemble magnetization can be written as [32]

$$M_u(H_u^A, T) = \frac{1}{\langle V \rangle} \int \mu F\left(\frac{\mu_0 \mu H_u^A}{kT}\right) f(\mu) d\mu, \quad (13)$$

where $\langle V \rangle$ is the mean NP volume, i.e., the NPs total volume divided by n_{ps} , and $F(\frac{\mu_0 \mu H_u^A}{kT})$ is a function of state, monotonous on H_u^A/T , whose form depends on $\nu = KV/kT$ and on the distribution of NP easy axes orientations relative to the applied field direction [28]. For $\nu \ll 1$, $F \approx L(\frac{\mu_0 \mu H_u^A}{kT})$, the Langevin function. For $\nu \gg 1$ and easy axes oriented along field direction, $F \approx \tanh(\frac{\mu_0 \mu H_u^A}{kT})$. These two situations correspond to the shadowed areas in Fig. 1. When the NPs experience magnetic dipolar interactions H_u^E is the effective field $H_u^A - N_u^E M_u(H_u^A, T)$, where N_u^E is the effective demagnetizing factor in the measurement direction \hat{u} . In this case Eq. (13) becomes a transcendental equation for $M_u(H_u^A, T)$:

$$M_u(H_u^A, T) = \frac{1}{V} \int \mu F\left(\frac{\mu_0 \mu (H_u^A - N_u^E M_u)}{kT}\right) f(\mu) d\mu. \quad (14)$$

Therefore, magnetization is no longer described by a superposition of $F(\frac{\mu_0 \mu H_u^A}{kT})$ functions. Nevertheless, when moments are unblocked such simple description allows satisfactory fitting of experimental results [20,21]. This observation leads to the following approximate relationship:

$$M_u(H_u^A, T) \approx \frac{1}{V_a} \int \mu_a F\left(\frac{\mu_0 \mu_a H_u^A}{kT}\right) g(\mu_a) d\mu_a. \quad (15)$$

In the last term, V_a and μ_a are apparent values of V and μ , respectively, and g is the distribution of μ_a values. In order that the approximate equality be of general validity, it would be necessary that

$$\mu_a \approx \mu(1 - N_u^E M_u/H_u^A).$$

Since μ_a and μ are not proportional to each other through a constant factor, f and g must have different mathematical forms. Moreover, μ_a is a multivalued function of μ since it depends on M_u/H_u^A . However, at a given T and within the range of H_u^A values where the recorded low field susceptibility $\chi_u = M_u/H_u^A$ can be considered constant, $\mu = (\chi_u/\kappa_u)\mu_a$ and both distributions become related by

$$g(\mu_a) = \frac{\chi_u}{\kappa_u} f\left(\frac{\chi_u}{\kappa_u} \mu_a\right), \quad (16)$$

where $\chi_u = \kappa_u/(1 - N_u^E \kappa_u)$ is the “true” NPs equilibrium susceptibility [Eq. (1)], i.e., the one which would be measured in the absence of interparticle interactions. Since χ_u/κ_u is a constant, μ_a is a single valued function of μ and both distributions have the same shape. Note that always $\chi_u \geq \kappa_u$, therefore g has a higher maximum than f and this maximum is located at a smaller moment value. Besides, for NPs in the unblocked regime, when $T \rightarrow 0$, $\chi_u \rightarrow \infty$, $\kappa_u \rightarrow 1/N_u^E$, and therefore $\kappa_u/\chi_u \rightarrow 0$. From $\mu_a = \kappa_u/\chi_u \mu$ it follows that $\mu_a \rightarrow 0$. Hence, an incorrect analysis of the equilibrium

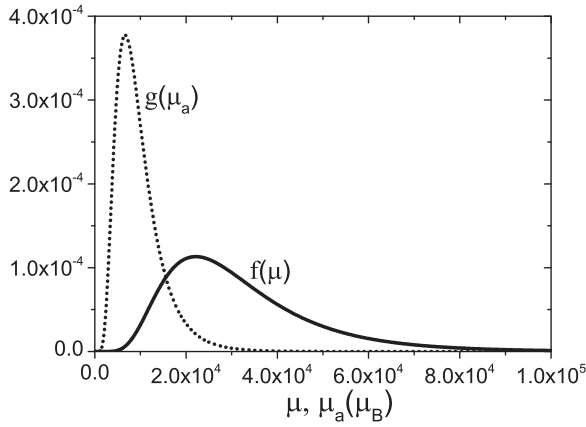


FIG. 5. Comparison of distribution functions f and g appearing in Eq. (16) for the case $\chi_u/\kappa_u = 10/3$. Lognormal distribution has been used.

response of an ensemble of interacting NPs, disregarding demagnetizing effects, leads to a nonphysical result: the NP mean apparent moment seems to approach a null value when temperature decreases, as it has been previously observed [20,21,33]. This artifact is clearly expressed by Eq. (16). Figure 5 illustrates the relationship between f and g for the arbitrary case $\chi_u/\kappa_u = 10/3$ and assuming a lognormal distribution of moments.

C. Demagnetizing factor and susceptibility

Several parameters appearing in Eq. (11) are usually known or can be retrieved from experiment while some others are unknown and need to be calculated using this equation and other relationships. Frequently, the specimen geometry is known and so N_{sx} , N_{sy} , and N_{sz} can be readily calculated. N_x^E , N_y^E , and N_z^E , are accessible using experimental protocols that will be described below. Reasonable estimations for the values of φ and φ_c can be made from studies of packing fraction of hard spheres in ordered (crystalline) and disordered arrays for cases of monodisperse and polydisperse spheres [34,35]. In cubic crystalline monodisperse materials φ ranges from 0.52 (single cell) to 0.74 (face centered cell). In disordered polydisperse systems φ takes a wide range of values and may attain much higher ones. It has been reported that packing fraction is a rapidly growing function of polydispersity and approaches 0.7 when polydispersity is about 0.4 [36]. The ensembles of NPs and clusters that will be discussed later present this order of polydispersity, therefore we will assume $\varphi = \varphi_c = 0.7$. This idealized situation leaves us with five unknowns N_{cx} , N_{cy} , N_{cz} , γ , and γ_c . This system can be solved using Eq. (11) for each principal direction, Eq. (12), and the relationship among NPs volume fraction x_V , packing fractions, and relative distances:

$$\gamma^3 \gamma_c^3 = \frac{\varphi \varphi_c}{x_V}. \quad (17)$$

Now we discuss an experimental protocol to determine N_x^E , N_y^E , and N_z^E . The equivalent of Eq. (1) for the ensemble of NPs under consideration is $1/\kappa_u = 1/\chi_u + N_u^E$. When NPs

are in thermal equilibrium, this expression becomes

$$\frac{1}{\kappa_u} = \frac{k}{\mu_0 V} \left(\frac{T}{\zeta_u(\nu) M S^2} \right) + N_u^E,$$

where Eq. (3) was used. The true low-field susceptibility χ_u can be retrieved from magnetization measurements of the original sample performed above the blocking temperature T_B , provided that NPs, in the isolated condition, would also have an equilibrium response. Then, plotting the inverse of low field susceptibility κ_u as a function of $T/\zeta M S^2$, N_u^E and true susceptibility $\chi_u = \frac{\kappa_u}{1+N_u^E \kappa_u}$ can be determined. From $\chi_u = \frac{\mu_0 \zeta_u(\nu) V M S^2}{k T}$, $\zeta(\nu) V$ can be obtained.

Frequently there is a distribution $f(\mu)d\mu$ of NP moments μ that cannot be ignored. We analyze how this distribution modifies our last expression. To this end, we study its effect on the equilibrium magnetization,

$$\begin{aligned} M_u(H_u^A, T) &= \frac{1}{\langle V \rangle} \int \mu F \left[\frac{\mu_0 \mu (H_u^A - N_u^E M_u(H_u^A, T))}{k T} \right] f(\mu) d\mu, \end{aligned}$$

where $\langle \rangle$ stands for mean value with the f distribution. Susceptibility in low-field limit is calculated from previous expression,

$$\begin{aligned} \kappa_u &= \frac{1}{\langle V \rangle} \int \frac{\zeta_u \mu_0 \mu^2 (1 - N_u^E \kappa_u)}{k T} f(\mu) d\mu \\ &= \frac{\mu_0}{k T \langle V \rangle} (1 - N_u^E \kappa_u) \langle \zeta_u \mu^2 \rangle. \end{aligned}$$

Solving for κ_u and writing its inverse,

$$\frac{1}{\kappa_u} = \frac{k \langle V \rangle}{\mu_0} \left(\frac{T}{\langle \zeta_u(\nu) \mu^2 \rangle} \right) + N_u^E. \quad (18)$$

Estimation of a useful approximated expression for $\langle \zeta_u(\nu) \mu^2 \rangle$, in the general case of an arbitrary distribution of NP easy axes orientations will be treated elsewhere [27]. In the particular case where easy axes are randomly oriented, Eq. (18) leads to

$$\frac{1}{\kappa_u} = \frac{3k}{\mu_0 \langle V \rangle} \left(\frac{T}{\rho M S^2} \right) + N_u^E, \quad (19a)$$

where $\rho = \langle \mu^2 \rangle / \langle \mu \rangle^2$. From Eq. (16) we notice that

$$\begin{aligned} \langle \mu_a^n \rangle &= \int \mu_a^n g(\mu_a) d\mu_a = \frac{\chi_u}{\kappa_u} \int \mu_a^n f\left(\frac{\chi_u}{\kappa_u} \mu_a\right) d\mu_a \\ &= \left(\frac{\chi_u}{\kappa_u} \right)^n \langle \mu^n \rangle, \end{aligned}$$

which leads to $\langle \mu_a^2 \rangle / \langle \mu_a \rangle^2 = \langle \mu^2 \rangle / \langle \mu \rangle^2 = \rho$, i.e., ρ can be evaluated using apparent moment μ_a and distribution g , from the analysis of M_u versus H_u^A measurements, which constitutes a convenient straightforward procedure. Then χ_u (and $\langle V \rangle$) as well as N_u^E can be obtained by measuring κ_u and M^S at different temperatures T . In terms of specimen susceptibility κ_{su} and specimen saturation magnetization M_s^S ,

$$\frac{1}{\kappa_{su}} = \frac{3k}{\mu_0 \langle V_{pp} \rangle} \left(\frac{T}{\rho M_s^S} \right) + N_{su}^E, \quad (19b)$$

where V_{pp} is the average volume per particle in the specimen, $V_{pp} = \frac{V_s}{n_{ps}}$, being n_{ps} the number of particles in the specimen and V_s the specimen volume.

Figure 13 illustrates the application of Eq. (19a) for a dispersion of magnetite NPs in a PVA hydrogel. $1/\kappa_u$ was plotted in terms of $\frac{T}{\rho M^2 S^2}$ for a wide temperature range. The straight line which best fits the part of the experimental data corresponding to NP moments in thermal equilibrium is shown. Vertical axis intercept is N_u^E , and $\langle V \rangle$ is retrieved from slope. When $N_u^E = 0$, $\kappa_u = \chi_u$ and Eq. (19a) becomes $\frac{1}{\chi_u} = \frac{3k}{\mu_0 \langle V \rangle} \left(\frac{T}{\rho M^2 S^2} \right)$ as expected for the susceptibility of noninteracting NPs with random distribution of easy axes, $\chi_u = \frac{\mu_0 \langle \mu^2 \rangle}{3kT \langle V \rangle}$. Note that this analysis only holds if the specimen is in thermodynamic equilibrium. Data points recorded out of this condition may depart from the linear behavior of Eq. (19a) as shown in Fig. 13.

D. Dipolar energy

The specimen average magnetic dipolar energy per NP, i.e., the interaction energy of one NP with the field produced by the others, when magnetization is measured in the direction \hat{u} of the applied field can be written as

$$\varepsilon_u = -\mu_0 \langle \vec{\mu}_i \cdot \vec{H}_i \rangle = \mu_0 N_u^E M_u^2 \langle V \rangle, \quad (20)$$

with N_u^E given by Eq. (11a). For simplicity we have disregarded correlations and approximated [37] $\langle \vec{\mu}_i \cdot \vec{H}_i \rangle \approx \langle \vec{\mu}_i \rangle \cdot \langle \vec{H}_i \rangle$, set $\langle \vec{\mu}_i \rangle = \langle V \rangle \vec{M}$ and $\langle \vec{H}_i \rangle = -N_u^E \vec{M}$. ε_u is different when specimen is magnetized in different directions. For same value of M , ε_u increases with N_u^E . It is convenient to explore ranges of values of ε_u for the typical situations that are encountered when dealing with NPs of common magnetic materials, such as Fe, Co, Ni, and their ferrites. Figure 6 displays ε_u for the cases corresponding to the demagnetizing factors illustrated in Fig. 4, assuming spherical NPs with $D = 10$ nm, and for an arbitrarily chosen magnetization

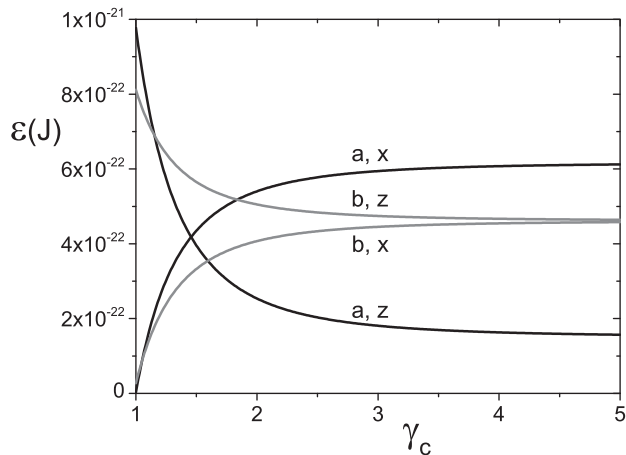


FIG. 6. Dipolar energy per NP for specimens whose demagnetizing factors are illustrated in Figs. 4(a) and 4(b) (identified by the scripts a and b respectively). x and z identify the magnetization direction. A value of $M = 10^5$ A/m has been used for the calculation.

$M = 10^5$ A/m, i.e., roughly midway toward saturation. ε_u is calculated for \vec{M} pointing in x and z directions.

Values of ε_u shown in Fig. 6, which correspond to quite concentrated clusters ($\gamma = 1.5$) of 10-nm diameter NPs, are of the order of 10^{-22} J to 10^{-21} J. According to Eq. (20) ε_u is proportional to M^2 , therefore in experiments aimed to determine the magnetic susceptibility κ_u where $M \ll M^S$ (frequently $M = 10^4$ A/m), ε_u takes values one or two orders of magnitude smaller than those shown in Fig. 6. ε_u also decreases rapidly with D and γ due to its cubic dependence on these quantities. For the typical ensembles of NPs just considered ε_u becomes of the order of kT for temperatures in the range 10–100 K.

For experiments performed under low applied field, where $M_u \approx \kappa_u H_u^A$, dipolar energy per NP can be approximated by $\varepsilon_u \approx \mu_0 N_u^E \kappa_u^2 H_u^A{}^2 V = \mu_0 N_u^E [\chi_u / (1 + N_u^E \chi_u)]^2 H_u^A{}^2 V$. Therefore, under a given applied field intensity, ε_u presents a maximum for $N_u^E \approx 1/\chi_u$. When the same field is applied along two different principal directions x, z , the ratio of low field susceptibilities recorded in those directions is

$$\frac{\varepsilon_x}{\varepsilon_z} \approx \frac{N_x^E M_x^2}{N_z^E M_z^2} = \frac{N_x^E \kappa_x^2}{N_z^E \kappa_z^2} = \frac{N_x^E}{N_z^E} \left[\left(\frac{\chi_x}{\chi_z} \right) \frac{1 + N_z^E \chi_z}{1 + N_x^E \chi_x} \right]^2, \quad (21)$$

which reduces to $\frac{\varepsilon_x}{\varepsilon_z} \approx \frac{N_x^E}{N_z^E} \left(\frac{1 + N_z^E \chi}{1 + N_x^E \chi} \right)^2$, in the case of random easy axes orientation, i.e., when $\chi_x = \chi_z = \chi$. In this case, Eq. (21) predicts that $\frac{\varepsilon_x}{\varepsilon_z} \approx 1$ for $\chi \approx (N_x^E N_z^E)^{-1/2}$. In terms of global specimen quantities, ε_u can be written as

$$\varepsilon_u = \mu_0 N_{su}^E M_{su}^2 V_{pp}.$$

The last expression can be derived in a straightforward manner from Eq. (20).

E. Comparison with model of Allia *et al.* [20]

The procedure described in Sec. II C is similar to one previously proposed by Allia *et al.* [20]. However, one important improvement is that adimensional parameter α introduced in that article can now be identified in terms of the effective demagnetizing factor. Allia *et al.* arrived at an equation [38] equivalent to Eq. (19b) of present work, which in the SI of units can be rewritten as $\frac{1}{\kappa_{su}} = \frac{3k}{\mu_0 \langle V_{pp} \rangle} \left(\frac{T}{\rho M_s^2} \right) + \frac{3\alpha}{\rho}$. Comparison of both expressions leads to the relationship $\frac{3\alpha}{\rho} = N_{su}^E$.

The model presented here uncovers that α is a function of specimen and cluster geometries, and that its value depends on specimen orientation during measurement of susceptibility. Therefore, it becomes clear that in order to make a meaningful comparison of susceptibility and dipolar energy results obtained from magnetic nanodispersions, a detailed description of specimen and measurement-conditions geometries must be given. Furthermore, it becomes clear the convenience of measuring magnetic properties along one of the specimen principal directions. There is still a question to be addressed. In the situation where moments are unblocked the model presented here as well as the one presented by Allia *et al.* propose modifications of the argument of the equilibrium function describing the magnetization, in order to give account of dipolar interaction between NPs. For the

simple case of monodisperse samples, and when NP anisotropy effects can be ignored, magnetization is well described by $M_{su}(H_u^A, T) = M_s^S(T)L(x)$, where $x = \mu_0\mu H_u^A/kT$ and L is the Langevin function. The two approaches propose modifications on temperature or field, as follows:

$$\begin{aligned} \text{no interaction} &\rightarrow \text{interaction} \\ x = \frac{\mu_0\mu H_u^A}{kT} &\rightarrow x = \frac{\mu_0\mu H_u^A}{k(T + T^*)} \\ &= \frac{\mu_0\mu H_u^A}{kT_{\text{eff}}} \text{ (Allia et al. [20]),} \\ x = \frac{\mu_0\mu H_u^A}{kT} &\rightarrow x = \frac{\mu_0\mu(H_u^A - N_{su}^E M_{su})}{kT} \\ &= \frac{\mu_0\mu H_u^E}{kT} \text{ (present work).} \end{aligned}$$

In the linear response regime ($x \ll 1$) both approaches are equivalent provided that

$$\begin{aligned} kT^* &= \frac{\mu_0\mu^2 N_{su}^E}{3kV_{pp}} \Rightarrow kT^* = \alpha \frac{\mu_0\mu^2}{4\pi d^3} \text{ (SI),} \\ kT^* &= \alpha \frac{\mu^2}{d^3} \text{ (cgs),} \end{aligned}$$

where $V_{pp} = V/x_V$, which can be set equal to d^3 when clusters are not considered, in agreement with definitions made in Ref. [20]. Therefore, both approaches are equivalent when the NP dispersion is uniform and $x \ll 1$. However, they are not equivalent at finite values of x because modifications are introduced either in the denominator or the numerator of x , depending on the approach. In consequence, the modification produced by adding T^* to denominator of x would lead to undesired deviations of the behavior of calculated $M(H, T)$, especially for $x \approx 1$. There is another difference with the description of Allia *et al.* In their formulation ε depends just on α , μ , and d values and is therefore independent of the specimen state of magnetization. In the present model ε depends on M^2 [Eq. (20)], which is a function of H^E and T , as it happens also for homogeneous materials. In Allia *et al.* model, dipolar energy per NP is estimated [20] as

$$\varepsilon = \frac{\alpha\mu_0\mu^2}{4\pi d^3}, \quad (22)$$

having α been observed to take values mostly in the interval 1–20. Equation (22) produces quite large values of ε , usually in the range of 10^{-21} to 10^{-20} J, which are similar to the ones obtained with Eq. (20) for nearly magnetic saturated states. As an example to illustrate this point we will calculate dipolar energy with both expressions for a single case: a $\text{Co}_{10}\text{Cu}_{90}$ inhomogeneous alloy containing 10.6 nm Co NPs separated on the average 18.7 nm, for which $\mu \approx 7.78 \times 10^4 \mu_B$ and $\alpha = 10.4$ (alloy identified as “2” in Ref. [20]). We use $\varphi = 0.7$ and will assume that specimen has a demagnetizing factor $N_{su}^E = 0.2$ in the direction of measurement, and that it is magnetized to saturation ($M^S \approx 1.4 \times 10^6$ A/m). Dipolar energy per NP evaluated with Eq. (20) leads to $\varepsilon_1 \approx 3.9 \times 10^{-20}$ J, while evaluated with Eq. (22) leads to $\varepsilon_2 \approx 8.4 \times 10^{-20}$ J independently of its magnetization state. Therefore, ε_2 is larger than ε_1 for any possible magnetization state.

We have demonstrated that the approximation based on the appearance of a demagnetizing field $-N_{su}^E M_{su}$ presented here is straightforward, brings information on specimen internal structure, produces a more reasonable estimation of dipolar interaction energy, and provides a reliable description of the material magnetic response for any value of H^A .

F. Conclusions and final considerations about the model

In conclusion, with the help of the model introduced here intrinsic properties of the magnetic NPs such as χ_u , $\langle V \rangle$, and $\langle \mu(T) \rangle$ as well as structural information of their spatial dispersion like relative distances γ , γ_c and demagnetizing tensor components N_{cu} and N_u^E can be obtained, while dipolar energy per NP can be estimated. This model, as the Allia *et al.* one does, gives account of two well-documented experimental observations: the increasing importance of dipolar interaction effects as γ (or d) decreases, and the observation of apparent NP magnetic moments, which approach zero as temperature approaches zero. However, the model presented here has a direct relation with the demagnetizing effect of dipolar interactions usually observed in NPs random solid dispersions. In addition, it brings a more complete physical description of dipolar interactions effects, by taking into account specimen shape and internal structure. By this way it is able to explain observed changes of specimen magnetization easy axis direction as γ_c decreases, for example, from those corresponding to cluster shape to that associated to specimen shape [23]. Its application allows the recovery of true values of NP magnetic moment and susceptibility. Model also leads to an expression for the mean dipolar energy per NP, which depends on magnetization and measurement directions. This predicted property of dipolar energy may lead to a dependence of NP Néel relaxation-process on experiment geometry.

The structural information provided by the present model on the spatial distributions of nanoparticles and clusters, and on clusters preferential orientation, could be a good complement to results obtained with frequently employed structural techniques as, for example, SANS, SAXS, DLS, TEM, SEM, among others.

Since our model describes NPs and clusters on the basis of spherical shapes, systematic errors should appear when aspect ratio of these entities becomes pronounced, for example, in specimens constituted for parallel arrangements of micrometer-long magnetic nanowires. However, we had performed preliminary analyses of the model predictions for some of these cases and found that it gives a reasonable qualitative and semiquantitative description of the ensemble properties.

III. EXPERIMENTAL RESULTS

A. Complementary interpretation of reported results

The aim of this section is to verify the ability of our model to retrieve information on the specimens structure, in particular on NPs and clusters distributions, and to test its consistence with the study performed by other authors. We will discuss results published by Allia and Tiberto [12] on oleic-acid-coated magnetite NPs in the form of dried powder (specimen named DP), and of solid dispersions in PEGDA-600 polymer

TABLE I. Values of NP volume fraction (x_V) calculated from data reported in Ref. [12], NP diameter reported in Ref. [40] (D') and obtained in the present work (D), mean interparticle distances reported in Ref. [12] (d') and obtained in the present work (d), effective demagnetizing factor (N_u^E), and relative distances γ and γ_c .

| Specimen | x_V | D' (nm) | D (nm) | d' (nm) | d (nm) | N_u^E | γ | γ_c |
|-------------------|-------------------------|-----------|----------|-----------|----------|----------|----------|------------|
| Dried Powder (DP) | 0.046(5) | 9.8 | 9.2(3) | 20 | 17(1) | 0.031(5) | 1.9(1) | 1.2(1) |
| PEG5 | $2.7(3) \times 10^{-4}$ | 8.2 | 8.2(3) | 16 | 13(1) | 0.054(7) | 1.6(1) | 7.4(4) |
| PEG10 | $5.5(5) \times 10^{-4}$ | 8.2 | 8.3(3) | 14 | 12(1) | 0.09(1) | 1.4(1) | 6.9(3) |
| PEG90 | 0.0046(5) | – | 17(2) | 29 | 25(3) | 0.073(4) | 1.5(1) | 3.2(1) |

with NP mass fractions $x_m = 0.0015, 0.003, 0.027$ (specimens named PEG5, PEG10, and PEG90). In connection with the model introduced here, these materials have the convenient feature that NPs are nearly spherical and monodisperse, to the extent that isothermal anhysteretic M versus H curves could be well described using a single Langevin function, thus making analysis and comparisons more simple. According to authors, NP diameters are about 8 nm and oleic acid shells have thicknesses of about 2 nm. They have measured isotherm M_s versus H^A curves for temperatures between 10 and 300 K, from which they have obtained initial (low field) susceptibility values κ , NP moments μ , and mean number of NPs per unit volume. They have plotted the equivalent of Eq. (19b) considering $\rho = 1$, in view of the very low size dispersion, and have determined T^* values. From their published data we have retrieved values of temperature, specimen susceptibility, and saturation magnetization, using information provided by Figs. 3 and 4 of Ref. [12], and converting magnetic magnitudes from cgs system to SI. We have estimated NP volume fractions as $x_V = M_s^S(300 \text{ K})/M^S(300 \text{ K})$ using $M^S(300 \text{ K}) = 375 \text{ kA/m}$ obtained from Ref. [12]. Since $M_s^S(300 \text{ K})$ is not reported we have obtained it by performing the ratio of T to $T/M_s^{S^2}$ from data presented in Figs. 3 and 4 of Ref. [12]. Finally, we have calculated NPs susceptibility κ_u and magnetization $M = M_s/x_V$.

N_u^E and D were obtained for each specimen by fitting the linear region (high temperature) of the experimental relationship between $1/\kappa_u$ and $T/(M^S)^2$ using Eq. (19a); see Fig. 1 in Supplemental Material [39]. Table I displays the values of x_V , N_u^E , D , d , γ and γ_c . It also displays NP diameters D' and distances d reported in Ref. [40]. D and D' values are in good agreement within estimated uncertainties. It is striking that size obtained for NPs in PEG90 specimen is too large, about twice that of NPs in the original dried powder. This result is in agreement with the values of NP magnetic moment reported in Ref. [12]. Allia and Tiberto came to the conclusion that magnetic individuality of NPs is lost in this specimen. In effect, PEG90 NPs present a moment about 20 times larger than the average NP one. In fact, they have observed clusters of about 40 nm in SEM micrographs taken on PEG90. They conclude that in this specimen (although not in the others) magnetic response is no longer determined by individual NPs but by NP aggregates. We will come back later to this point.

Now we will calculate γ , γ_c , and d for each of the specimens using some reasonable assumptions. For PEG specimens we make the reasonable simplifying assumption that clusters are randomly oriented which leads to $N_{cu} \approx 1/3$ for any direction. In the case of DP specimen there are no differentiated clusters,

hence we may consider the specimen as a single cluster satisfying $\varphi_c = 1$. From Eqs. (11a) and (17) the following expression for γ is obtained:

$$\gamma = \left[\frac{\varphi}{3N_u^E - x_V(3N_{su} - 1)} \right]^{1/3}. \quad (23)$$

Since N_u^E and x_V were already calculated and the estimation $\varphi \approx 0.5$ was made for PEG specimens, Eq. (23) gives γ as a function of N_{su} . In all of these cases γ varies less than 2.1% within the whole range of N_{su} allowed values. By considering usual experimental limitations, good practices for magnetic measurements, and requests expressly indicated by magnetometer makers, we can safely assume that $0.1 \leq N_{su} \leq 0.33$. γ and its uncertainty were calculated taking $N_{su} = 0.2(1)$. The lack of correlation between γ and N_{su} strongly suggests that NPs are organized in clusters which interact weakly with each other, therefore specimen shape became almost irrelevant.

Once γ is obtained, mean distance d between near neighbor particles can be calculated. Good agreement between d values obtained with our model and those reported in Ref. [12] (d') is observed in Table I.

Now γ_c can be calculated using Eq. (17). γ and γ_c are plotted for all of the PEG solid dispersions in Fig. 7 (the value corresponding to DP specimen is indicated by an arrow for completeness). The tendency to clustering is confirmed by the evolution of both relative distances parameters. On one

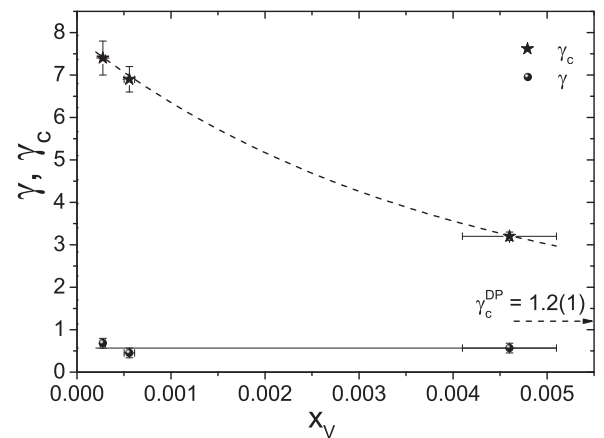


FIG. 7. Relative interparticle distances, γ , and intercluster distances, γ_c , as a function of volume fraction x_V for all PEG specimens listed in Table I. The value corresponding to DP specimen is indicated by an arrow for completeness.

hand, NP interdistance remains small and almost unchanged ($1.4 < \gamma < 1.6$) for all of the PEG specimens, indicating that NPs always are close to each other. On the other hand, γ_c decreases from about 7.5 (PEG5) to about 3.2 (PEG90), indicating that clusters become closer to each other due to increasing NP concentration. Allia *et al.* state that Fig. 1(b) of Ref. [12] shows NP clusters with $D_c \approx 40$ nm in PEG90. Since $\gamma_c \approx 3.2$ for this specimen, mean separation between near-neighbor clusters should be $d_c = \gamma_c D_c \approx 130$ nm, which is in reasonable agreement with separations observed in the same figure. For DP specimen $\gamma = 1.9(1)$ and $\gamma_c = 1.2(1)$ consistently with a powder specimen with no clusters as shown in Fig. 1(a) of Ref. [12].

In conclusion, the comparison of results obtained by the application of our model to data reported in Ref. [12], with the structural parameters reported in that reference, is satisfactory. In addition, our model not only gives account for clustering effects in PEG specimens, but allows the estimation of relative intercluster distances γ_c . For specimen PEG90 the estimated mean separation of $d_c \approx 130$ nm is consistent with SEM image shown in Fig. 1(b) of Ref. [12]. The fact that magnetic response of PEG90 (NP moment value) corresponds to entities larger than NPs used in the preparation of this solid dispersion is intriguing. Especially because this is not the case for PEG5 and PEG10 specimens, where clustering also occurs, and almost with the same interparticle separation. One possibility is that oleic acid coating of at least a fraction of the NPs is missing in PEG90 specimen, allowing exchange interactions between them and the formation of sort of magnetic domains larger than NPs themselves.

B. Study of hydrogel (PVA) and magnetic nanoparticles Fe_3O_4 ferrogels

In this section we present an experimental study of PVA and Fe_3O_4 ferrogels. Experimental details are given in Sec. III B 1. In Sec. III B 2 the procedure indicated in Sec. II C is followed in order to obtain intrinsic information on NPs properties such as mean volume $\langle V \rangle$, as well as true susceptibility χ_u , spontaneous magnetization M^S , ρ , and NP mean true moment μ as function of temperature. By application of Eq. (19a), N_u^E is also retrieved for one principal direction. This information together with knowledge of x_V and N_{su} values, estimation of φ , φ_c , and experimental determination of κ_u at room temperature in three principal directions for several specimens, is used in Sec. III B 3 to obtain extrinsic properties, such as γ , γ_c , the three N_{cu} , and N_u^E in the two remaining principal directions.

1. Specimens and procedures

Magnetic characterization was performed using MPMS XL-7 SQUID from Quantum Design and 7304 VSM from LakeShore.

Ferrogel samples whose preparation is described in the Supplemental Material [39] were kindly provided by collaborators [41]. The samples were named FGXPi where X is the nominal NP mass percentage and Pi identifies different specimens with prism shape with dimensions l_x , l_y , and l_z . Characters a and b identify two samples obtained through two synthesis processes with same NP mass concentration and different NP volume

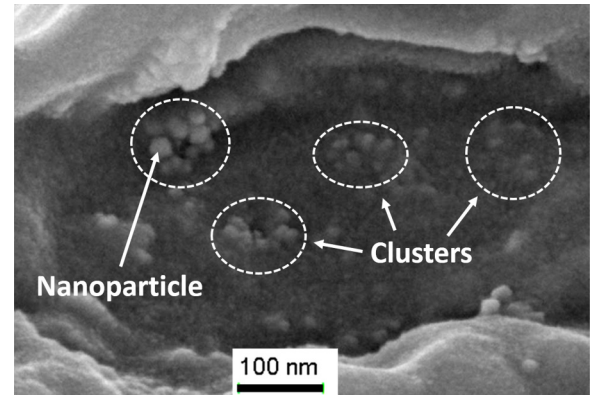


FIG. 8. FESEM image of FG6 specimen. Clusters of NPs are indicated.

fraction. Samples used in this work have five different NP volume fractions (see Table II). A field emission scanning electron microscopy (FESEM) image from a cryofractured surface of FG6 sample is shown in Fig. 8 where aggregates of NPs can be observed.

Specimens were cut from ferrogel foils with rectangular prism shapes, with $l_x > l_y \gg l_z$, in order to allow the identification of the principal directions and the calculation of N_{su} . Linear dimensions were kept under 5 mm in order to fulfill VSM and SQUID technical requirements. Demagnetizing factors associated with specimen geometry, calculated in the three prism principal directions using the expression given in Ref. [42], are listed in Table II.

Measurements in the SQUID were carried out on FG9aP1 specimen with the applied field pointing along x direction. M versus H^A cycles were recorded varying field in the interval $[-6$ T, 6 T] at different temperatures between 10 and 300 K. Warming part of ZFC and FC measurements were performed under a field of 0.01 T; and cooling part of ZFC and TRM measurements were performed with no applied field. All of them were carried out in the range between 10 and 300 K. FG9aP1 specimen was measured first in its dry state and then in a completely hydrated state. In the second case, during the final part of the ZFC measurement and the initial part of the FC protocol, temperatures were kept below water liquefaction point in order to avoid potential out-of-equilibrium melting-freezing phenomena. SQUID experimental window time for $M(H^A)$ measurements was estimated to be about 100 s.

Measurements in the VSM were M versus H^A cycles at room temperature at applied fields between -1.9 and 1.9 T. They were performed on all of the specimens with field applied in the x , y , and z directions. Sensor coils are located on the pole ends and have a diameter of ~ 8 mm. Magnetic poles diameter is 100 mm and gap between poles was set to 22 mm. VSM experimental window time was estimated to be about 30 s.

2. Determination of NPs intrinsic properties

ZFC-FC results obtained with the SQUID for FG9aP1 specimen, processed to subtract diamagnetic signal from PVA and water, are shown in Fig. 9. Field was applied parallel to the longest (l_x) prism dimension. It can be noticed that κ_x is

TABLE II. Specimens FGXPi (see text), NPs volume fractions x_V , rectangular prism dimensions l_x , l_y , and l_z , and specimen shape demagnetizing factors (calculated according to Ref. [42])

| Specimen | x_V | l_x (mm) | l_y (mm) | l_z (mm) | N_{sx} | N_{sy} | N_{sz} |
|----------|-----------|------------|------------|------------|----------|----------|----------|
| FG1P3 | 0.0017(1) | 4.00(2) | 2.00(2) | 0.12(2) | 0.036(4) | 0.074(9) | 0.89(1) |
| FG3P7 | 0.0067(4) | 4.68(2) | 1.32(2) | 0.24(2) | 0.046(3) | 0.17(1) | 0.78(1) |
| FG6P6 | 0.0158(8) | 4.90(2) | 1.10(2) | 0.20(2) | 0.037(3) | 0.17(1) | 0.79(1) |
| FG9aP1 | 0.0169(9) | 4.00(2) | 2.00(2) | 0.14(2) | 0.040(4) | 0.083(9) | 0.88(1) |
| FG9aP5 | | 4.90(2) | 1.00(2) | 0.14(2) | 0.028(4) | 0.15(1) | 0.83(2) |
| FG9bP2 | 0.020(1) | 3.90(2) | 3.00(2) | 0.24(2) | 0.066(3) | 0.087(5) | 0.847(9) |
| FG9bP4 | | 5.00(2) | 1.00(2) | 0.24(2) | 0.040(2) | 0.21(1) | 0.75(1) |

larger for hydrated than for dry sample. This is consistent with the expected effect of hydration, i.e., due to materials swelling distances among magnetic NPs and/or clusters should increase thus reducing demagnetizing effects and increasing measured susceptibility.

Equation (19a) was applied to results obtained from dry specimen. To this end a temperature range where the specimen is in thermodynamic equilibrium during the process of data acquisition was selected. This interval was identified by the coincidence of ZFC and FC responses which begins at the irreversibility temperature T_{irr} . A close inspection of Fig. 9 (see inset) reveals that $240 \text{ K} \leq T_{irr} \leq 250 \text{ K}$. In order to apply Eq. (19a), $\rho = \langle \mu^2 \rangle / \langle \mu \rangle^2$ and M^S were also determined. To this end, analysis of cycles M versus H^A measured at different temperatures for FG9aP1 specimen (Fig. 10) was performed, after removal of the minor diamagnetic contribution originated essentially from PVA, using [the equivalent of Eq. (15)]

$$M(H^A, T) \approx \frac{1}{\langle V_a \rangle} \int \mu_a L\left(\frac{\mu_0 \mu_a H^A}{kT}\right) g(\mu_a) d\mu_a, \quad (24)$$

where we have used a Lognormal distribution as $g(\mu_a)$ and approximated $F \approx L$ disregarding, for the sake of simplicity, possible effects of finite values of $\nu = KV/kT$. Such

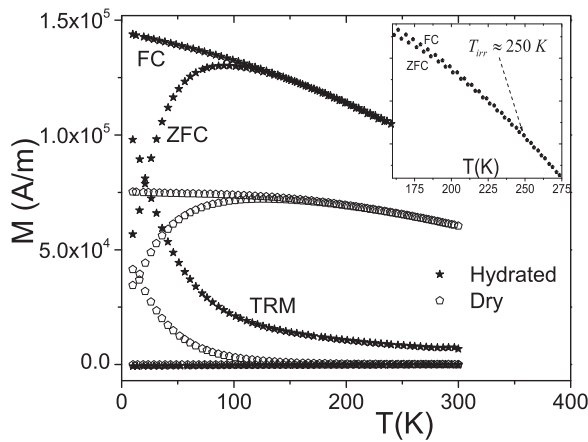


FIG. 9. ZFC-FC-TRM curves from FG9aP1 specimen. Cooling part of ZFC and TRM measurements were performed under zero field. Warming part of ZFC and FC measurements were performed under a 8 kA/m field. Field was applied parallel to the longest (l_x) prism dimension. Inset shows a close look of ZFC-FC around irreversible temperature (T_{irr}) of dry specimen

approximation should be acceptable when $\nu \leq 3$ (see Fig. 2(b) in Ref. [28]), which corresponds to $T \geq 250 \text{ K}$ assuming typical values of K for magnetite NPs of about 10 nm. No coercivity is observed at $T = 300 \text{ K}$, which is the only measurement performed above 250 K (inset of Fig. 10). From these analyses, values of M^S and ρ were determined for each temperature, which are presented in Figs. 11 and 12 (dots). ρ and M^S temperature dependence were fitted with a linear function and $M^S(T) = A(1 - T/B)^C$, respectively, in order to have continuous expressions for $\rho(T)$ and $M^S(T)$ suitable for the analysis of κ_x results [Eq. (19a)]. Then, $1/\kappa_x$ (ZFC and FC) was plotted as a function of $T/\rho M^S$ (see Fig. 13).

A departure from linear behavior becomes evident below 215 K, this departure becoming more pronounced at lower temperatures. This behavior is reasonably consistent with the fact that reversibility holds only above 240–250 K. From the analysis of the linear region with Eq. (19a) values of $N_x^E = 0.068(1)$ and $\langle V \rangle = 1.15(2) \times 10^3 \text{ nm}^3$ ($D = 13.0(1) \text{ nm}$ assuming spherical NPs), were estimated. The knowledge of N_x^E is important because it allows to retrieve susceptibility values corresponding to noninteracting NPs, as $\chi_x = \kappa_x / (1 - N_x^E \kappa_x)$. Figure 14 displays κ_x and the result calculated for χ_x using the previous expression as a function of temperature. χ_x is represented with filled or open spheres, identifying

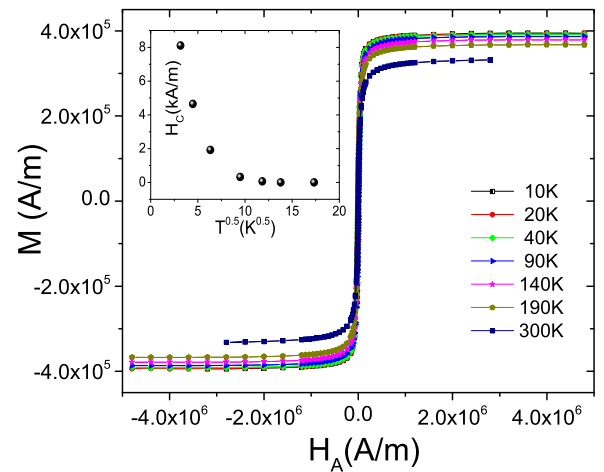


FIG. 10. $M(H^A)$ cycles for FG9aP1 specimen at several temperatures. Field was applied parallel to the longest (l_x) prism dimension. Inset shows coercive field (H_c) vs. temperature.

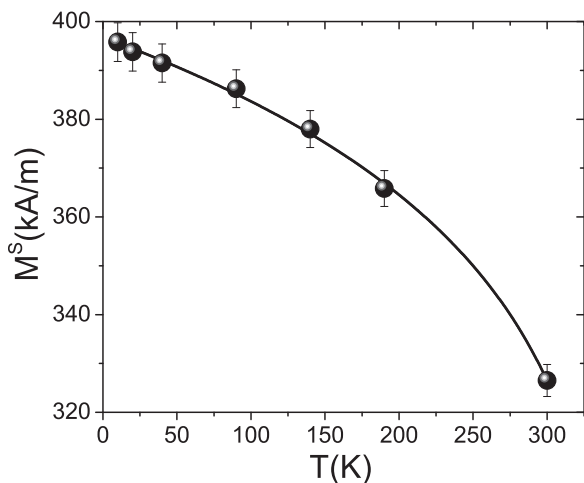


FIG. 11. Saturation magnetization M^S versus temperature T for FG9aP1 specimen. Dots were obtained from the analysis of Fig. 10 data. Line corresponds to fitting with $M^S(T) = A(1 - T/B)^C$. The values obtained were $A = 3.97(1) \times 10^2$ kA/m, $B = 350(8)$ K, and $C = 0.100(7)$

temperature regions where specimen is in- or out-of-equilibrium, respectively. These regions are separated by a vertical dashed line. Correction in the equilibrium region is supported by the procedure outlined in this work, in which just the equilibrium susceptibility term was considered in Eq. (19a). Notice in Fig. 14 that after correcting for demagnetizing effects, room temperature susceptibility increases 2.8(2) times to a value $\chi_x(300 \text{ K}) = 26(2)$.

Considering the procedures followed when preparing the materials studied in this section, a random distribution of NP easy axes is expected, therefore we can safely assume that $\chi_x \approx \chi_y \approx \chi_z$. Increase of susceptibility with diminution of dipolar interactions is readily observed from experimental results, by comparing specimen responses in dried and completely

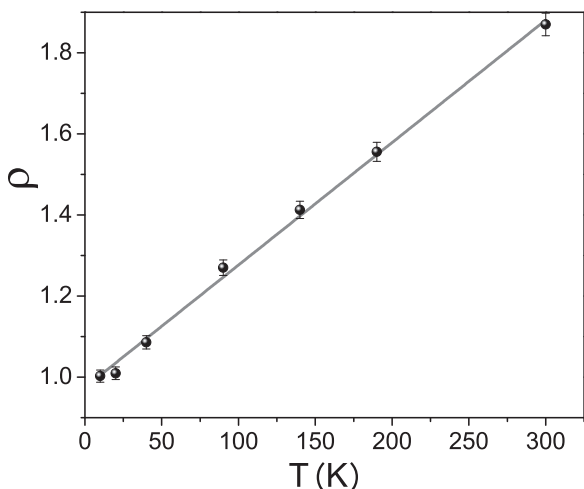


FIG. 12. $\rho = \langle \mu^2 \rangle / \langle \mu \rangle^2$ versus temperature T were μ is the NP magnetic moment. Dots were obtained from the analysis of Fig. 10 data. Line corresponds to fitting with a linear function $\rho = AT + B$. The values obtained were $A = 3.1(1) \times 10^{-3} \text{ K}^{-1}$ and $B = 0.97(1)$.

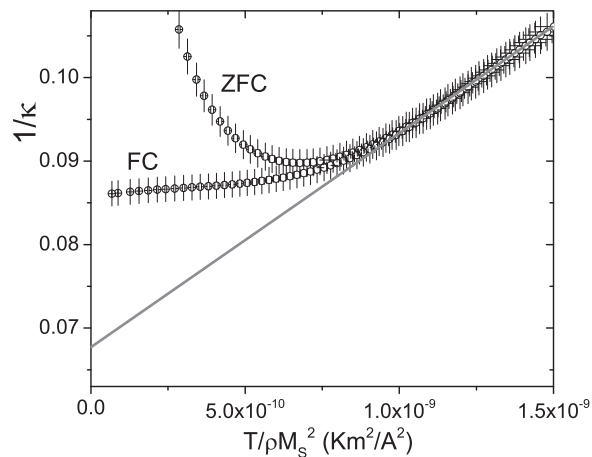


FIG. 13. Inverse of apparent susceptibility $1/\kappa_x$, obtained from ZFC and FC measurements, as a function of $T/\rho M_s^2$. Straight line is the fit of the linear region (specimen magnetization in thermal equilibrium).

hydrated states. Hydration increases susceptibility maximum by a factor of about 1.44. This increase is explained by the fact that hydration expands the PVA matrix and pulls apart NPs and NP clusters, reducing dipolar interactions. It can be seen that hydration also produces a temperature shift of the maximum-susceptibility temperature, from 126 to 91 K (see Fig. 9). This shift is not accounted for by the transformation $\chi_x = \frac{\kappa_x}{1 - N_x^E \kappa_x}$ when κ_x is the in-phase component of the apparent susceptibility. In this regard it is convenient to remark that the estimation of χ_x is valid at temperatures at which the system is in equilibrium. This expression should hold between complex susceptibilities [Eq. (2), even out-of-equilibrium] in absence and presence of dipolar interactions whose incidence on NP moment relaxation times needs to be studied. It has been widely reported that dipolar interactions produce an increase of τ [11], and it is well documented that temperatures at which susceptibility maximum and blocking occurs, frequently increase with increasing relaxation time.

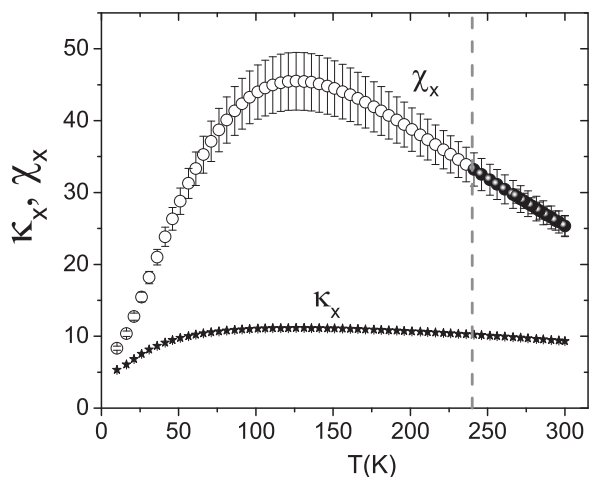


FIG. 14. Apparent susceptibility κ_x and corrected (true) susceptibility χ_x . Vertical dash line corresponds to $T = T_{irr}$, therefore correction is only reliable at $T \geq T_{irr}$ (black symbols for χ_x).

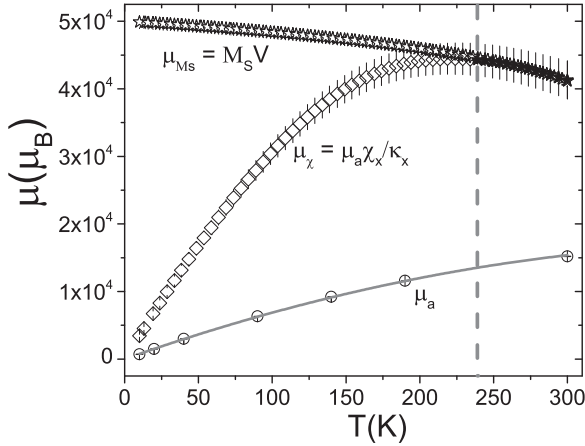


FIG. 15. NP magnetic moment μ : μ_a is the apparent NP moment, μ_χ is the corrected NP moment obtained with the present model, and μ_{Ms} is the NP moments obtained through saturation magnetization data. Vertical dash line corresponds to $T = T_{ir}$, therefore correction μ_χ is only reliable at $T \geq T_{ir}$ (black-star symbols).

NP apparent mean moment μ_a obtained from fits with Eq. (24) of cycles shown in Fig. 10 is represented in Fig. 15 (filled spheres in bottom curve) as a function of temperature. Continuous line represents interpolated values obtained with a quadratic function. Notice that μ_a displays a nonphysical behavior since its value increases with temperature. Following Sec. II A we have corrected μ_a NP moment, using susceptibility results, to $\mu_\chi = (\frac{\chi_u}{\kappa_u})\mu_a$. Again we have used filled symbols (stars) to distinguish the equilibrium temperature region from the out-of-equilibrium one (open stars). Another way of recovering true NP mean moments is from saturation magnetization measurement, as $\mu_{Ms} = M^S \langle V \rangle$, where $\langle V \rangle = 1.15(2) \times 10^3 \text{ nm}^3$ was previously determined. μ values obtained in this way are also represented in Fig. 15. In the temperature region where equilibrium holds ($T \geq 240 \text{ K}$) the relation $\mu_\chi \approx \mu_{Ms}$ also holds, supporting the present model.

Equation (20) states that dipolar energy per NP (ϵ) depends on magnetization and on effective demagnetizing factor, i.e., takes different values when experiment is performed along different specimen axes. It reaches values of about 1.0×10^{-20} and $2.2 \times 10^{-20} \text{ J}$ when our specimens are magnetized to saturation along their longest and shorter dimensions, respectively. For ZFC-FC experiments ϵ values were of at most $5.5 \times 10^{-22} \text{ J}$.

3. Parameters of NPs space distribution: Effective demagnetizing factor and demagnetizing factors of clusters

Figure 16 displays specific magnetization curves $\sigma(H^A)$ [43] of specimen FG6P6 obtained at room temperature with a VSM, after removal of diamagnetic contribution. Field was applied along the three principal prism directions (see Table II). It can be observed that high-field magnetization appears to follow $\sigma_x > \sigma_y > \sigma_z$. This effect, observed in all of the specimens, is an artifact originated in the measurement geometry (finite size sample and sample geometry effects [44,45]). When external field is applied in the x direction, for example, a larger fraction of the stray field lines originated at specimen magnetization come across the VSM sensing coils

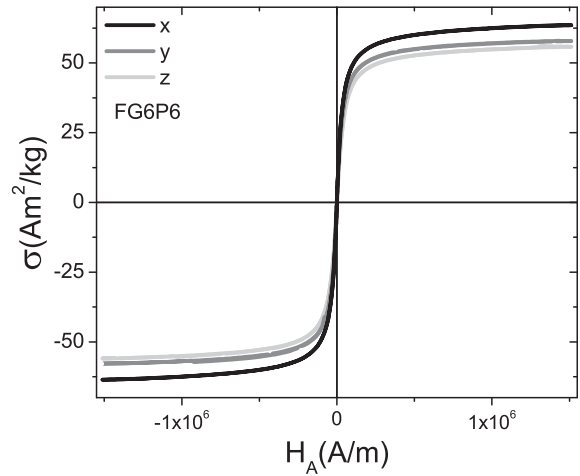


FIG. 16. $\sigma(H)$ cycles for specimen FG6P6 (raw data).

than when external field is applied in any other direction. Therefore, due to these geometrical conditions, flux Φ across sensing coils satisfies $\Phi_x > \Phi_y > \Phi_z$ leading to the observed effect. For subsequent analysis these cycles were normalized at high fields taking as reference the one obtained at room temperature using the SQUID (Fig. 10). Figure 17 shows the linear (central) region of the normalized $M(H^A)$ cycles for specimen FG9aP1. The low-field apparent susceptibilities were obtained from the analysis of this region and are listed in Table III for all of the specimens. Only specimen FG1P3 presents a small coercivity of at most 350 A/m (4.4 Oe) revealing that a small fraction of NPs is not in equilibrium. For all specimens $\kappa_x > \kappa_y > \kappa_z$ (except for FG3P7 where $\kappa_x \approx \kappa_y > \kappa_z$), as listed in Table III. This is connected to demagnetizing effects originated, at least partially, in specimen geometry. In effect, since $l_x > l_y > l_z$, then $N_{sx} < N_{sy} < N_{sz}$. This could in turn lead to $N_x^E < N_y^E < N_z^E$ and to the observed result. Figure 18 displays the dependence of κ_u on N_{su} for all of the specimens in the three measured directions.

As already mentioned, all of the specimens have been synthesized using commercial NPs from the same batch, and

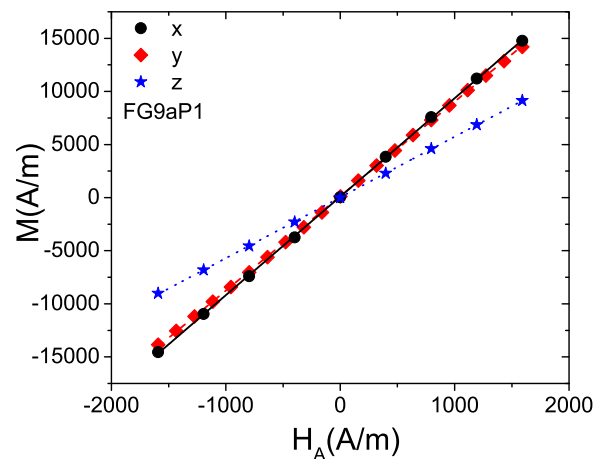


FIG. 17. Linear region of $M(H)$ curves, measured in FG9aP1 specimen with the applied field along the three prism directions. Curves were normalized at high fields as described in the text.

TABLE III. Susceptibilities κ_u measured in the three prism directions $u = x, y, z$. Relative distance parameters γ and γ_c . Specimen effective demagnetizing factors N_{su}^E . Demagnetizing factors N_{cu} associated to average cluster shape.

| Specimen | κ_x | κ_y | κ_z | γ | γ_c | N_x^E | N_y^E | N_z^E | N_{cx} | N_{cy} | N_{cz} |
|----------|------------|------------|------------|----------|------------|----------|----------|----------|----------|----------|----------|
| FG1P3 | 9.7(2) | 9.6(2) | 6.5(2) | 1.42(1) | 4.6(2) | 0.063(2) | 0.065(2) | 0.115(5) | 0.26(1) | 0.27(1) | 0.47(2) |
| FG3P7 | 8.6(2) | 8.6(2) | 5.9(2) | 1.35(1) | 3.1(1) | 0.077(3) | 0.076(3) | 0.129(6) | 0.28(1) | 0.28(1) | 0.45(2) |
| FG6P6 | 8.7(2) | 8.5(2) | 6.0(2) | 1.35(1) | 2.32(8) | 0.076(3) | 0.079(3) | 0.128(6) | 0.29(1) | 0.29(1) | 0.44(2) |
| FG9aP1 | 9.3(2) | 8.9(2) | 5.7(2) | 1.36(1) | 2.25(8) | 0.068(2) | 0.073(3) | 0.135(6) | 0.27(1) | 0.28(1) | 0.48(2) |
| FG9aP5 | 9.1(2) | 9.0(2) | 5.8(2) | 1.37(1) | 2.25(8) | 0.070(3) | 0.072(3) | 0.132(6) | 0.28(1) | 0.28(1) | 0.47(2) |
| FG9bP2 | 8.7(2) | 8.4(2) | 5.4(2) | 1.33(1) | 2.19(7) | 0.076(3) | 0.080(3) | 0.144(7) | 0.27(1) | 0.29(1) | 0.47(2) |
| FG9bP4 | 8.6(2) | 8.4(2) | 5.5(2) | 1.33(1) | 2.18(7) | 0.076(3) | 0.080(3) | 0.143(7) | 0.28(1) | 0.28(1) | 0.47(2) |

isotropic distributions of NP easy axes are expected from ferrogels fabrication procedure. Therefore, noninteracting susceptibility should be the same in all specimens and directions, i.e., $\chi_x \approx \chi_y \approx \chi_z \approx \chi$.

From Eqs. (1), (11), (17), and $\text{Tr}(N_u^E) = \frac{\phi}{\gamma^3}$, the unknowns N_u^E , N_{cu} , γ , and γ_c are obtained. To calculate the corresponding uncertainties all expressions were written as function of the known parameters x_V , N_{sx} , N_{sy} , N_{sz} , and of the measured apparent susceptibilities. Results are listed in Table III and displayed in Figs. 19 and 20.

Figure 19 clearly reflects the organization of NPs in clusters. In effect, values of γ indicate that mean separation between near neighbor NPs is $d \approx 1.35D$. Since particles have a polyacrylic acid coating, such separation is consistent with NPs in contact or in a near contact configuration, similar to that observed in Fig. 8. In fact, a close inspection of that micrograph indicates that average size of coated NP is about 17 nm, in good agreement with $D \approx 13$ nm, obtained in the previous section. On the other hand, Fig. 19 shows that clusters separation monotonously decrease with NPs volume fraction. FESEM image shown in Fig. 8 correspond to FG6 sample and shows clusters of the order of 70 nm separated by distances of about 150–160 nm, consistently with results in Table III and Fig. 18 ($\gamma_c \approx 2.3$). Mean cluster distance increases up to almost 4.6 times the cluster size in the case of FG1 specimen. Figure 20 indicates that N_{cu} factors are not too far from 1/3, the value expected in the case of a random distribution of

cluster orientations. However, N_{cz} displays a clear tendency to stay above 1/3. This result suggests a nonrandom distribution of clusters orientation. In support of last interpretation it may be recalled that ferrogel fabrication procedure introduces asymmetries. Since z is always the direction normal to ferrogel foils surface, nonisotropic clusters may have acquired a degree of texture during ferrogel formation and drying. After drying in Petri dishes, ferrogel samples are several centimeters in diameter but only one or two tenths of millimeters thick.

The linear region of $M(H^A)$ curves was corrected for demagnetizing effects by the usual transformation from (H^A, M) coordinates to $(H^E = H^A - N_u^E M, M)$ ones. Figure 21 displays the corrected results for all specimens studied in the present work. It is worth mentioning that VSM field stability is of the order of 1–2 Oe (80–160 A/m). In almost all of the cases the M versus H^E curves overlap to each other within the field uncertainty. Only the results from one specimen (FG1P3) depart systematically from the rest by at most 350 A/m (4.4 Oe). This small coercivity was observed also in the (H^A, M) representation of FG1P3 magnetization (not shown). Such agreement is expected because demagnetizing correction does not affect coercivity.

C. Summary of experimental section

We have applied this model to PEG-magnetite and PVA-magnetite nanocomposites with different NP volume fractions between 0.0017 and 0.05. Analysis of susceptibility

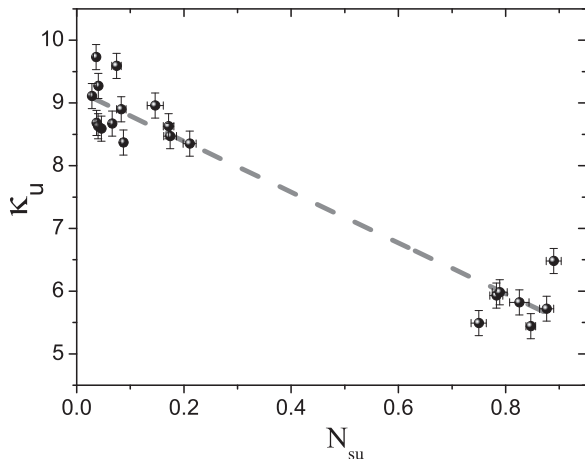


FIG. 18. Measured (apparent) susceptibilities κ_u versus demagnetizing factors N_{su} corresponding to specimen shape.

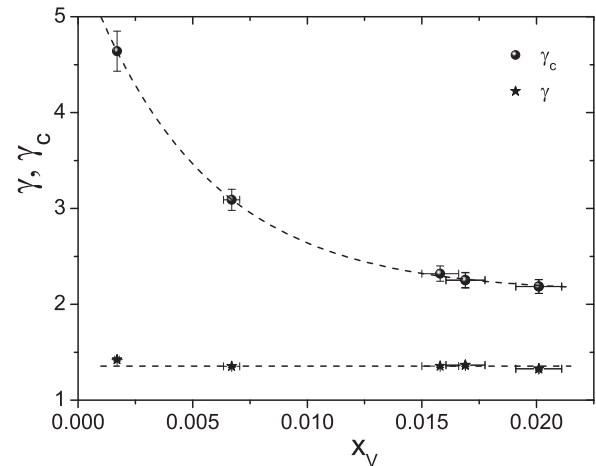


FIG. 19. Relative distance parameters γ and γ_c versus NPs volume fraction x_V .

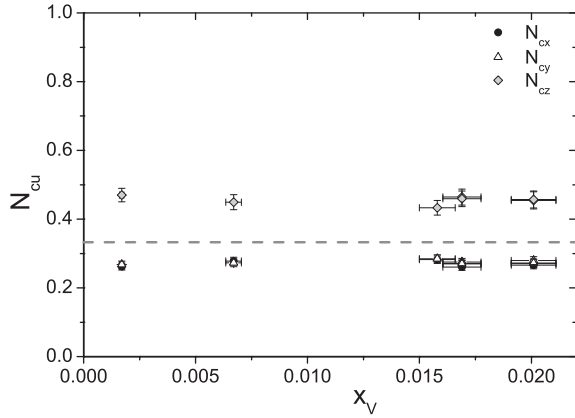


FIG. 20. Cluster demagnetizing factors N_{cu} , as a function of NPs volume fraction x_V . Dashed line stands for the expected value for random cluster orientations, $N_{cu} = 1/3$.

measurements furnished quantitative information on clustering occurrence and was consistent with clusters being quasirandomly oriented in all of the samples. Retrieved interparticle relative distances were $1.4 \leq d/D \leq 1.6$ in PEG-magnetite specimens and $1.3 \leq d/D \leq 1.4$ in PVA-magnetite specimens. Taking into account that NPs have a few nanometers of polyacrylic acid coating, these results indicate that NPs are in close contact to each other. Relative intercluster distances were found to be in the ranges $3.2 \leq d_c/D_c \leq 7.5$ and $2.2 \leq d_c/D_c \leq 4.6$ in PEG-magnetite and PVA-magnetite specimens, respectively. Hence, NPs should be almost exclusively in aggregates. These results were supported by FESEM observations.

IV. CONCLUSIONS AND REMARKS

One of the highlights of the MFISP model introduced here is that it is simple and practical. It allows the retrieval of relevant information about the NPs spatial distribution through the relative distances γ and γ_c , and cluster demagnetizing factors N_{cx} , N_{cy} , and N_{cz} . It also allows the estimation of

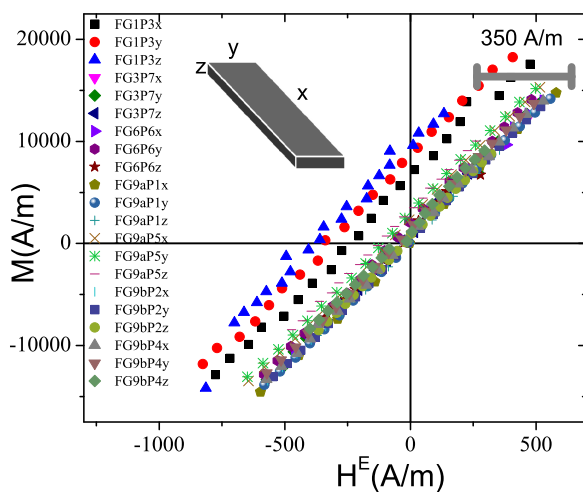


FIG. 21. Linear part of room temperature M vs. H^E cycles for all of the specimens, after correcting by demagnetizing effects.

dipolar energy per NP and makes explicit its dependence on specimen shape and magnetization state.

Its application requires the occurrence of experimental conditions, which are frequently fulfilled. In its actual formulation, its main limitations are connected with shape and distribution of NP clusters. As relative cluster distance $\gamma_c = d_c/D_c$ decreases and becomes comparable to unity its application should lead to nonnegligible systematic deviations of the values of retrieved parameters. It must be remarked that in its present form the model does not describe the effects of dipolar interactions on NP magnetic moment relaxation, and therefore its application must be constrained to conditions where the ensemble of NP magnetic moments is in thermal equilibrium, i.e., it behaves like an interacting superparamagnet.

From its formulation and application, it becomes evident that magnetic measurements of sufficiently concentrated NP ensembles must be designed taking into account specimen geometry and directions along which external field is applied and magnetic properties are measured. In this regard, we consider it useful to introduce protocols aimed to organize and simplify experiments devoted to retrieving information from such ensembles. In order to determine NPs intrinsic properties it is necessary to apply Eq. (19b), which implies that M_s , ρ , and κ_u must be previously determined as functions of temperature. To this end, it is suggested to measure M versus H^A , at different temperatures, and to obtain the mentioned quantities from fitting whole or part of the cycles with appropriate functions and distributions. Alternatively, κ_u can be obtained from ZFC-FC measurements under low enough applied fields, with the advantage of making this magnitude available as a quasicontinuous function of T . If random orientation of NP moment easy axes is expected, experimental determination of κ_u versus T can be made along just one specimen principal direction \hat{u} ; otherwise, measurements must be performed along the three principal directions. Having determined the mentioned quantities, χ_u and $\langle V \rangle$ are readily determined using Eq. (19b) (this procedure also leads to the determination of the effective demagnetizing factor N_{su}^E). Then, true NP mean magnetic moment can be retrieved as a function of temperature by using $\langle \mu \rangle(T) = M^S(T) \langle V \rangle$.

In order to retrieve the rest of extrinsic properties, the set of Eq. (11a) must be used. To this end, apparent magnetic susceptibility κ_u must be known in the three specimen principal directions \hat{u} at just one temperature in order to obtain the remaining effective demagnetizing factors from $N_u^E = \frac{1}{\kappa_u} - \frac{1}{\chi_u}$. Application of Eq. (11a) also requires knowledge of x_V , φ , and φ_c . Usually x_V can be accurately estimated from synthesis data and experimental determination of material density. Packing factors φ and φ_c can be reasonably estimated by observing that theory, experiment, and simulations indicate that they should be within 0.52 and 0.85 for mono and polydisperse arrangements of hard spheres in both ordered and disordered states. With this information γ , γ_c , and cluster demagnetizing factors N_{cu} can be determined.

ACKNOWLEDGMENTS

This research was funded by Grant No. PIP 11220110100720CO of CONICET and Grant No. 11/X680 of UNLP, Argentina. We thank Dr. Vera Álvarez, Dr.

Jimena González, and Eng. María Pía Areal, from Materiales Compuestos de Matriz Polimérica, INTEMA-UNMdP-

CONICET, Argentina, for providing ferrogel samples studied in Sec. III B.

-
- [1] J. Govan and Y. K. Gun'ko, Recent advances in the application of magnetic nanoparticles as a support for homogeneous catalysts, *Nanomaterials* **4**, 222 (2014).
- [2] V. K. Varadan, *Nanomedicine Design and Applications of Magnetic Nanomaterials, Nanosensors and Nanosystems* (Wiley, Chichester, UK, 2008).
- [3] K. Zargoosh, H. Abedini, A. Abdolmaleki, and M. R. Molavian, Removal of heavy metal ions from industrial wastes using thiosalicylhydrazide-modified magnetic nanoparticles, *Ind. Eng. Chem. Res.* **52**, 14944 (2013).
- [4] K. Komarek, M. Safarikova, T. Hubka, I. Safarik, M. Kandelova, and H. Kujalova, Extraction of alkylphenols and nonylphenol mono- and diethoxylates from water using magnetically modified adsorbents, *Chromatographia* **69**, 133 (2009).
- [5] M. Zayat, R. Pardo, G. Rosa, R. P. del Real, M. Diaz-Michelena, I. Arruego, H. Guerrero, and D. Levy, A Sol-Gel based magneto-optical device for the NANOSAT space mission, *J. Sol-Gel Sci. Technol.* **50**, 254 (2009).
- [6] Warner, *Magnetic Nanomaterials* (Wiley-VCH, Weinheim, 2009).
- [7] S. P. Gubin, Y. A. Koksharov, G. B. Khomutov, and G. Y. Yurkov, Magnetic nanoparticles: Preparation, structure and properties, *Russian Chem. Rev.* **74**, 489 (2005).
- [8] S. Hasany, N. Abdurahman, A. Sunarti, and R. Jose, Magnetic iron oxide nanoparticles: chemical synthesis and applications review, *Curr. Nanosci.* **9**, 561 (2013).
- [9] R. López-Ruiz, F. Luis, J. Sesé, J. Bartolomé, C. Deranlot, and F. Petroff, Zero-temperature spin-glass freezing in self-organized arrays of Co nanoparticles, *Europhys. Lett.* **89**, 67011 (2010).
- [10] B. Hillebrands, S. O. Demokritov, C. Mathieu, S. Riedling, O. Büttner, A. Frank, B. Roos, J. Jorzick, A. N. Slavin, B. Bartenlian, C. Chappert, F. Rousseaux, D. Decanini, E. Cambriil, A. Müller, and U. Hartmann, Arrays of interacting magnetic dots and wires: static and dynamic properties, *J. Magn. Soc. Japan* **23**, 670 (1999).
- [11] R. K. Das, S. Rawal, D. Norton, and A. F. Hebard, A collective dynamics description of dipolar interactions and the coercive field of magnetic nanoparticles, *J. Appl. Phys.* **108**, 123920 (2010).
- [12] P. Allia and P. Tiberto, Dynamic effects of dipolar interactions on the magnetic behavior of magnetite nanoparticles, *J. Nanopart. Res.* **13**, 7277 (2011).
- [13] G. T. Landi, The random dipolar-field approximation for systems of interacting magnetic particles, *J. Appl. Phys.* **113**, 163908 (2013).
- [14] R. Skomski, G. C. Hadjipanayis, and D. J. Sellmyer, Effective demagnetizing factors of complicated particle mixtures, *IEEE Trans. Magn.* **43**, 2956 (2007).
- [15] P. S. Normile, M. S. Andersson, R. Mathieu, S. S. Lee, G. Singh, and J. A. De Toro, Demagnetization effects in dense nanoparticle assemblies, *Appl. Phys. Lett.* **109**, 152404 (2016).
- [16] A. Aharoni, *Introduction to the Theory of Ferromagnetism* (Oxford University Press, Oxford, New York, 2000).
- [17] B. D. Cullity, *Introduction to Magnetic Materials* (IEEE/Wiley, Hoboken, NJ, 2009).
- [18] R. Yanes, O. Chubykalo-Fesenko, H. Kachkachi, D. A. Garanin, R. Evans, and R. W. Chantrell, Effective anisotropies and energy barriers of magnetic nanoparticles with néel surface anisotropy, *Phys. Rev. B* **76**, 064416 (2007).
- [19] C. Djurberg, P. Svedlindh, P. Nordblad, M. F. Hansen, F. Bødker, and S. Mørup, Dynamics of an Interacting Particle System: Evidence of Critical Slowing Down, *Phys. Rev. Lett.* **79**, 5154 (1997).
- [20] P. Allia, M. Coisson, P. Tiberto, F. Vinai, M. Knobel, M. A. Novak, and W. C. Nunes, Granular Cu-Co alloys as interacting superparamagnets, *Phys. Rev. B* **64**, 144420 (2001).
- [21] P. Mendoza Zélis, D. Muraca, J. S. Gonzalez, G. A. Pasquevich, V. A. Alvarez, K. R. Pirota, and F. H. Sánchez, Magnetic properties study of iron-oxide nanoparticles/PVA ferrogels with potential biomedical applications, *J. Nanopart. Res.* **15**, 1613 (2013).
- [22] In Ref. [20] the expression is written in the cgs system, $\varepsilon = \alpha\mu^2 d^3$; however, α is independent of the units system.
- [23] G. Kartopu, O. Yalcin, M. Es-Souni, and A. C. Bascaran, Magnetization behavior of ordered and high density Co nanowire arrays with varying aspect ratio, *J. Appl. Phys.* **103**, 093915 (2008).
- [24] K. Nielsch, R. B. Wehrspohn, J. Barthel, J. Kirschner, U. Gösele, S. F. Fischer, and H. Kronmüller, Hexagonally ordered 100 nm period nickel nanowire arrays, *Appl. Phys. Lett.* **79**, 1360 (2001).
- [25] G. Méridet, E. Dubois, M. Jardat, A. Bourdon, G. Demouchy, V. Dupuis, B. Farago, R. Perzynski, and P. Turq, Understanding the structure and the dynamics of magnetic fluids: Coupling of experiment and simulation, *J. Phys.: Condens. Matter* **18**, S2685 (2006).
- [26] J. I. Gittleman, B. Abeles, and S. Bozowski, Superparamagnetism and relaxation effects in granular Ni-SiO₂ and Ni-Al₂O₃ films, *Phys. Rev. B* **9**, 3891 (1974).
- [27] P. Mendoza Zélis *et al.* (unpublished).
- [28] J. Carrey, B. Mehdaoui, and M. Respaud, Simple models for dynamic hysteresis loop calculations of magnetic single-domain nanoparticles: Application to magnetic hyperthermia optimization, *J. Appl. Phys.* **109**, 083921 (2011).
- [29] C. P. Bean and J. D. Livingston, Superparamagnetism, *J. Appl. Phys.* **30**, S120 (1959).
- [30] M. Tejedor, H. Rubio, L. Elbaile, and R. Iglesias, External fields created by uniformly magnetized ellipsoids and spheroids, *IEEE Trans. Magn.* **31**, 830 (1995).

- [31] D. H. Han, J. P. Wang, and H. L. Luo, Crystallite size effect on saturation magnetization of fine ferrimagnetic particles, *J. Magn. Magn. Mater.* **136**, 176 (1994).
- [32] R. Chantrell, J. Popplewell, and S. Charles, Measurements of particle size distribution parameters in ferrofluids, *IEEE Trans. Magn.* **14**, 975 (1978).
- [33] M. E. de Sousa, M. B. F. van Raap, P. C. Rivas, P. M. Zélis, P. Girardin, G. A. Pasquevich, J. L. Alessandrini, D. Muraca, and F. H. Sánchez, Stability and relaxation mechanisms of citric acid coated magnetite nanoparticles for magnetic hyperthermia, *J. Phys. Chem. C* **117**, 5436 (2013).
- [34] C. Kittel, *Introduction to Solid State Physics* (Wiley, Hoboken, NJ, 2005).
- [35] E. I. Corwin, M. Clusel, A. O. N. Siemens, and J. Brujić, Model for random packing of polydisperse frictionless spheres, *Soft Matter* **6**, 2949 (2010).
- [36] K. W. Desmond and E. R. Weeks, Influence of particle size distribution on random close packing of spheres, *Phys. Rev. E* **90**, 022204 (2014).
- [37] As usually done in mean-field approximations.
- [38] Equation (11) of Ref. [20].
- [39] See Supplemental Material at <http://link.aps.org/supplemental/10.1103/PhysRevB.95.134421> for additional information on materials preparation and data treatment.
- [40] P. Allia, P. Tiberto, M. Coisson, A. Chiolerio, F. Celegato, F. Vinai, M. Sangermano, L. Suber, and G. Marchegiani, Evidence for magnetic interactions among magnetite nanoparticles dispersed in photoreticulated PEGDA-600 matrix, *J. Nanopart. Res.* **13**, 5615 (2011).
- [41] V. Álvarez, J. González, and M. Pía Areal, in *Materiales Poliméricos Termoplásticos INTEMA-UNMdP-CONICET*, Argentina.
- [42] A. V. Aharoni, Demagnetizing factors for rectangular ferromagnetic prisms, *J. Appl. Phys.* **83**, 3432 (1998).
- [43] σ is the NP magnetization given per unit mass of magnetite.
- [44] J. Lindemuth, J. Krause, and B. Dodrill, Finite sample size effects on the calibration of vibrating sample magnetometer, *IEEE Trans. Magn.* **37**, 2752 (2001).
- [45] A. Zieba, Image and sample geometry effects in SQUID magnetometers, *Rev. Sci. Instrum.* **64**, 3357 (1993).